



# Structure, electrical and optical properties of ZnO and Cu-doped ZnO films prepared by magnetron sputtering at different H<sub>2</sub> fluxes

Bailin Zhu<sup>1,\*</sup>, Xiaojian Cai<sup>1</sup>, Ming Xie<sup>1</sup>, Xinwei Shi<sup>2</sup>

<sup>1</sup>The State Key Laboratory of Refractories and Metallurgy, Wuhan University of Science and Technology, Wuhan 430081, People's Republic of China

<sup>2</sup>School of Physics and Microelectronics, Zhengzhou University, Zhengzhou 450001, People's Republic of China

Received 7 November 2023; Received in revised form 17 February 2024; Accepted 12 May 2024

## Abstract

Zn<sub>1-x</sub>Cu<sub>x</sub>O ( $x = 0$  and  $0.02$ ) films were prepared by RF magnetron sputtering in H<sub>2</sub>-containing atmosphere at 150 °C. Their structure and optical-electrical properties as functions of H<sub>2</sub> flux were investigated. With increase of H<sub>2</sub> flux, thickness of both films decreases and their surface roughness increases at first and then decreases. Preferred (002) orientation and improved crystallinity of both films were observed in specific interval of H<sub>2</sub> fluxes. With increasing H<sub>2</sub> flux, the V<sub>O</sub> content of ZnO and Cu-doped ZnO films decreases at first and then increases and decreases, respectively, but the Zn<sub>i</sub> content in both films increases at first and then decreases. Compared with ZnO films, Cu-doped ZnO films have lower V<sub>O</sub> and Zn<sub>i</sub> contents, and they maintain thicker film thickness and higher crystallinity at larger H<sub>2</sub> fluxes. Both films can obtain low resistivity in appropriate H<sub>2</sub> flux ranges, but their resistivity increases significantly after vacuum annealing. With increasing H<sub>2</sub> flux, intensity ratio of A<sub>1</sub>(LO) to E<sub>2</sub><sup>high</sup> scattering peaks, I(A<sub>1</sub>(LO))/I(E<sub>2</sub><sup>high</sup>), tends to increase, and scattering peaks around 135 and 185 cm<sup>-1</sup> appear. Compared with ZnO films, Cu-doped ZnO films can obtain lower resistivity, better electrically conductive stability in air, lower I(A<sub>1</sub>(LO))/I(E<sub>2</sub><sup>high</sup>) and smaller E<sub>g</sub>. High H<sub>2</sub> fluxes can cause decrease of T<sub>vis</sub> of the Cu-doped ZnO films. The influence mechanisms of introducing H<sub>2</sub> on microstructure and lattice defects of the films were discussed, and correlation between the optical-electrical properties of the films and the microstructure and lattice defects was analysed.

**Keywords:** Cu-doped ZnO, films, magnetron sputtering, electrical properties, optical properties

## I. Introduction

ZnO has a wurtzite crystal structure with a band gap ( $E_g$ ) of 3.37 eV and an exciton binding energy of 60 meV. As a functional material, ZnO has a wide range of applications in many fields such as light emitting diodes, photodetectors, surface acoustic wave, solar cells, transparent conductive films and gas sensors [1–3]. The lattice constant and band structure of the ZnO will be changed by doping, and optical, electrical and magnetic properties are modified accordingly [4,5]. Among dopants, Cu has the similar electronic shell structure and almost equal ionic radius as Zn, which leads to great interest for Cu-doped ZnO structures, especially films. At present, Cu-doped ZnO films have

exhibited attractive potential in tuning optical properties, achieving *p*-type conduction and realizing room temperature ferromagnetism [6–11]. On the other hand, hydrogen-doped ZnO films have also received special attention recently. This is because first-principles calculations show that hydrogen can have as a shallow donor role in ZnO [12,13]. Moreover, many experimental studies have confirmed that the incorporation of hydrogen into ZnO films is an effective method for improving electrical conductivity of ZnO films [14–17]. At the same time, the optical properties of ZnO films are also tailored with the incorporation of hydrogen.

In addition to single doping, co-doping has also been employed to further improve the optical and electrical properties of ZnO films. For example, the hydrogen and group III-A element co-doped ZnO films exhibit better transparent conductive properties even at

\*Corresponding author: tel: +86 27 68862529  
e-mail: blzhu@wust.edu.cn

room temperature (RT) [18,19]. For the hydrogen and Cu co-doped ZnO, the theoretical calculations have indicated that there is interaction between hydrogen and Cu and Cu–H defect complex may be formed in the ZnO [20–22]. Experimentally, there are currently few reports on structure and optical-electrical properties of Cu and hydrogen co-doped ZnO films. Zhou *et al.* [23] first prepared Cu-doped ZnO flakes ( $8 \times 8 \times 0.3 \text{ mm}^3$ ), and then implanted hydrogen ions into flakes to obtain Cu and hydrogen co-doped ZnO samples. The results showed that hydrogen ion implantation significantly increased the electrical conductivity of the flake (from  $4.67 \times 10^{-7}$  to  $1.5 \times 10^2 \Omega^{-1} \cdot \text{cm}^{-1}$ ). Li *et al.* [24] prepared Cu-doped ZnO films using pulsed laser deposition (PLD) technology, and then annealed them at  $500^\circ\text{C}$  in Ar(95%) + H<sub>2</sub>(5%) atmosphere for 1 h to obtain Cu and hydrogen co-doped ZnO films. The results showed that the A<sub>1</sub>(LO) scattering peak, ferromagnetism and green light emission peak of the Cu-doped ZnO film significantly enhanced, while its transmittance decreased after hydrogenation treatment at  $500^\circ\text{C}$ . For the hydrogenated films, the A<sub>1</sub>(LO) scattering peak and ferromagnetism decreased after annealing at  $500^\circ\text{C}$  in O<sub>2</sub> atmosphere, but the strong green light peak still existed after annealing at  $700^\circ\text{C}$  in O<sub>2</sub> atmosphere. Cai *et al.* [25] first prepared Cu-doped ZnO films by using metal-organic chemical vapour deposition (MOCVD) method, followed by the treatment in a high-pressure H<sub>2</sub> atmosphere to obtain Cu and hydrogen co-doped ZnO films. The results showed that the film transformed from high-resistance state to *n*-type conductivity ( $1.90 \times 10^2 \Omega \cdot \text{cm}$ ) after hydrogenation treatment. For the hydrogenated films, the resistivity remained in the range of  $3.28\text{--}5.77 \times 10^1 \Omega \cdot \text{cm}$  after annealing in N<sub>2</sub> atmosphere at  $400\text{--}750^\circ\text{C}$  for 30 min.

Although above sporadic reports have indicated that hydrogen and Cu co-doped ZnO films may exhibit some unique optical, electrical and magnetic properties, the studies on the influence of preparation process parameters on the structure and properties of co-doped films are not in-depth and systematic. For example, Zhou *et al.* [23] studied the electrical properties of co-doped films through impedance spectroscopy, but did not investigate the changes in film crystallinity, point defects and optical properties. The effects of H<sub>2</sub> content in the annealing atmosphere were not reported and the electrical properties of co-doped films were not investigated in the study of Li *et al.* [24]. In Cai *et al.* paper [25], the Raman spectra and transmittance properties of the Cu and hydrogen co-doped ZnO films were not studied. Furthermore, no one has investigated the hydrogen and Cu co-doped ZnO films prepared by other methods up to now. In order to further understand the doping behaviour of hydrogen and Cu in ZnO films, it is necessary to prepare the hydrogen and Cu co-doped ZnO films by new methods and investigate the structure and properties of the co-doped films as functions of processing parameters. Compared with the Cu and hydrogen co-doped

ZnO films obtained through post hydrogenation treatment mentioned above, introducing H<sub>2</sub> during preparation of the films can directly obtain co-doped films. As there is no need for further processing, this method is more convenient. Moreover, in this method, it is easy to achieve changes in doped hydrogen content by changing the H<sub>2</sub> flux.

In our recently published paper, the effects of introducing H<sub>2</sub> during sputtering and Cu doping on the structure and opto-electro-magnetic properties of ZnO films were investigated at a high substrate temperature ( $300^\circ\text{C}$ ) [26]. Meanwhile, the structure and optoelectronic properties of lightly Cu-doped (0.5 at.%) ZnO films prepared with different H<sub>2</sub> fluxes (0–15 sccm) at two substrate temperatures ( $150$  and  $300^\circ\text{C}$ ) were also investigated [27]. In this study, the hydrogen and Cu co-doped ZnO films were prepared by changing the H<sub>2</sub> flux (0–45 sccm) during sputtering with 2 at.% Cu-doped ZnO ceramics as the target at substrate temperature of  $150^\circ\text{C}$ . The structure (film thickness, preferred orientation, grain size, stress, surface roughness and point defects) and electrical-optical properties (electrically conductive properties, Raman spectra, transmittance,  $E_g$ , PL spectra) of the co-doped films as functions of H<sub>2</sub> flux were systematically and meticulously investigated. It was found that the results obtained were different from those of the co-doped films mentioned above, and the role of hydrogen doping in co-doped films was discussed accordingly. In addition to the study on Cu and hydrogen co-doped ZnO films, study on hydrogen-doped ZnO films was also carried out. Through comparative study, the role of Cu doping in co-doped ZnO films was also discussed. All obtained results provide a reference for the device application of the films.

## II. Experimental

### 2.1. Deposition of films

Zn<sub>1-x</sub>Cu<sub>x</sub>O ( $x = 0$  and  $0.02$ ) films were deposited by RF magnetron sputtering of previously prepared targets on thin soda-lime-silica glass substrates in H<sub>2</sub>-containing atmosphere at  $150^\circ\text{C}$ . The ZnO target was obtained by uniaxial pressing of ZnO powder (99.99% purity, Alfa Aesar) into a disc and subsequently sintering at  $1200^\circ\text{C}$  in air for 2 h, whereas the Zn<sub>0.98</sub>Cu<sub>0.02</sub>O target was prepared by compaction of ZnO and CuO (99.99% purity, Alfa Aesar) powder mixture weighed in stoichiometric ratio and sintering at  $1500^\circ\text{C}$  in air for 2 h. The relative densities of two obtained targets were about 95%, and their diameter and thickness were 60 and 6 mm, respectively. Before deposition, the soda-lime-silica glass substrates were cleaned in alcohol, acetone and distilled water successively in an ultrasonic cleaner for 15 min. The vacuum chamber was evacuated to  $1.0 \times 10^{-3}$  Pa, after which Ar and H<sub>2</sub> were introduced into the chamber as sputtering gases. The substrate temperature, RF power, sputtering pressure, deposition time and substrate-target distance were fixed at

150 °C, 150 W, 1.0 Pa, 30 min and 70 mm, respectively. Using mass flow controllers, the Ar flux was fixed at 50 sccm, whereas the H<sub>2</sub> flux was varied in the range of 0–45 sccm. The vacuum annealing process of the films was carried out under pressure of  $1 \times 10^{-3}$  Pa using the system of magnetron sputtering. Under the vacuum condition, the samples were heated from RT to a set temperature (150, 300 or 450 °C) at a rate of about 15 °C/min, and naturally cooled to RT after holding at the set temperature for 2 h.

## 2.2. Characterization

The film thickness was measured by an interference microscope (6JA, Shanghai Optical Instrument Factory). The crystalline structure of the films was identified by X-ray diffraction (XRD; Xpertpro, Philips) using Cu K<sub>α1</sub> radiation in  $\theta$ -2 $\theta$  Bragg-Brentano geometry. The surface morphology and roughness of the films were analysed by an atomic force microscope (AFM; SPM 5500, Agilent). The cross-section morphology of representative films was observed by FE-SEM (Nova 400 NanoSEM, FEI). The chemical compositions of the films and the chemical states of Zn, O and Cu in the films were investigated by X-ray photoelectron spectroscopy (XPS) on a photoelectron spectrometer (Axis Supra+, Kratos) using the Al K<sub>α</sub> excitation line (1486.6 eV). The binding energy was calibrated according to C 1s (284.8 eV) and all spectra were analysed by Avantage software. The electrical properties of the films were determined by Hall effect measurement using Van der Pauw method. The transmittance spectra of the films were obtained from an UV-visible spectrophotometer (UV-2102PC, Unico) in the wavelength range of 300–850 nm. The Raman spectra of the samples were recorded using a laser microscopic confocal Raman spectrometer (LabRam HR800, Horiba Jobin-Yvon), and a 532 nm lasers were used as an excitation source. All the above characterizations were performed at RT.

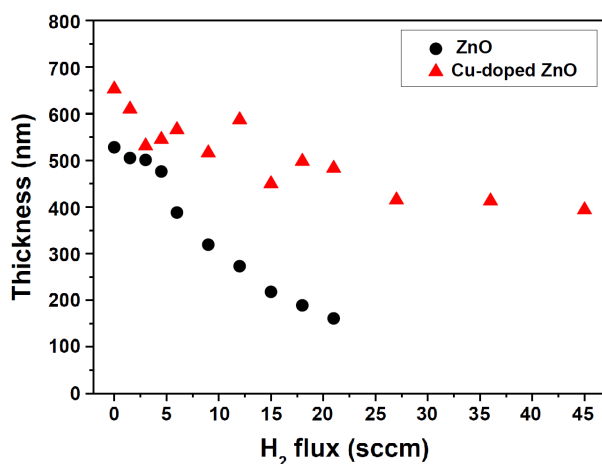


Figure 1. Thickness of the ZnO and Cu-doped ZnO films as a function of H<sub>2</sub> flux

## III. Results and discussion

### 3.1. Structural characterization

Figure 1 shows the thickness of the ZnO and Cu-doped ZnO films as a function of H<sub>2</sub> flux. It can be seen that the thickness of the ZnO film rapidly decreases from about 550 to 150 nm when the H<sub>2</sub> flux increases from 0 to 21 sccm. It can be expected that the film would become thinner if the H<sub>2</sub> flux is further increased. Since too thin film is unfavourable for the structure and optoelectronic properties analyses, the H<sub>2</sub> flux was chosen to be up to 21 sccm during deposition of ZnO films. For the Cu-doped ZnO films, the film thickness decreases slowly from about 650 to 400 nm when the H<sub>2</sub> flux increases from 0 to 45 sccm. Previous studies have also observed that the thickness of ZnO or doped ZnO films decreased with increasing H<sub>2</sub> flux [28–30], and there were two possible reasons: i) the introduction of H<sub>2</sub> dilutes Ar, which reduces the sputtering yield and ii) the active hydrogen species of the formed hydrogen plasma during the sputtering process had an etching effect on the ZnO-based films. At the same H<sub>2</sub> flux, the thickness of the Cu-doped ZnO films was obviously lower than that of the ZnO films.

As discussed above, the thickness of both ZnO and Cu-doped ZnO films decreases as the H<sub>2</sub> flux increases. One of the reasons for decrease of thickness is the etching effect of hydrogen plasma. The basic mechanism of etching is that hydrogen plasma undergoes an oxidation-reduction reaction with ZnO to generate metal Zn, which has a high saturation vapour pressure and is easily volatile. Compared to the metal Zn, Cu has much higher melting and boiling point, as well as a lower saturation vapour pressure. When Cu is present in the films, it may hinder the redox reaction between hydrogen plasma and ZnO, or hinder the volatilization of Zn. As a result, the etching effect of hydrogen plasma on ZnO is greatly slowed down, resulting in a larger thickness of the Cu-doped ZnO films. This is a reasonable speculation about this result at present, and further study is needed to confirm the underlying reasons.

Figure 2 shows XRD patterns of the ZnO and Cu-doped ZnO films prepared under different H<sub>2</sub> fluxes. From Fig. 2a, the ZnO films prepared under different H<sub>2</sub> fluxes show a hexagonal wurtzite structure. When the H<sub>2</sub> flux is 0–4.5 sccm, obvious diffraction peaks of ZnO (100) and (002) crystal planes appear in the films. When the H<sub>2</sub> flux is 6–18 sccm, the films only exhibit diffraction peak from (002) crystal plane, indicating that the film has a strong (002) preferred orientation. In general, the intensity of (002) diffraction peak shows a trend of first increasing and then decreasing with the increase of H<sub>2</sub> flux. From Fig. 2b, all diffraction peaks of the Cu-doped ZnO films come from the crystal plane of hexagonal wurtzite structured ZnO, and no diffraction peaks of other phases such as CuO and Cu<sub>2</sub>O are detected, which indicates that Cu is incorporated into the ZnO lattice. When the H<sub>2</sub> flux is 0 sccm, there are strong

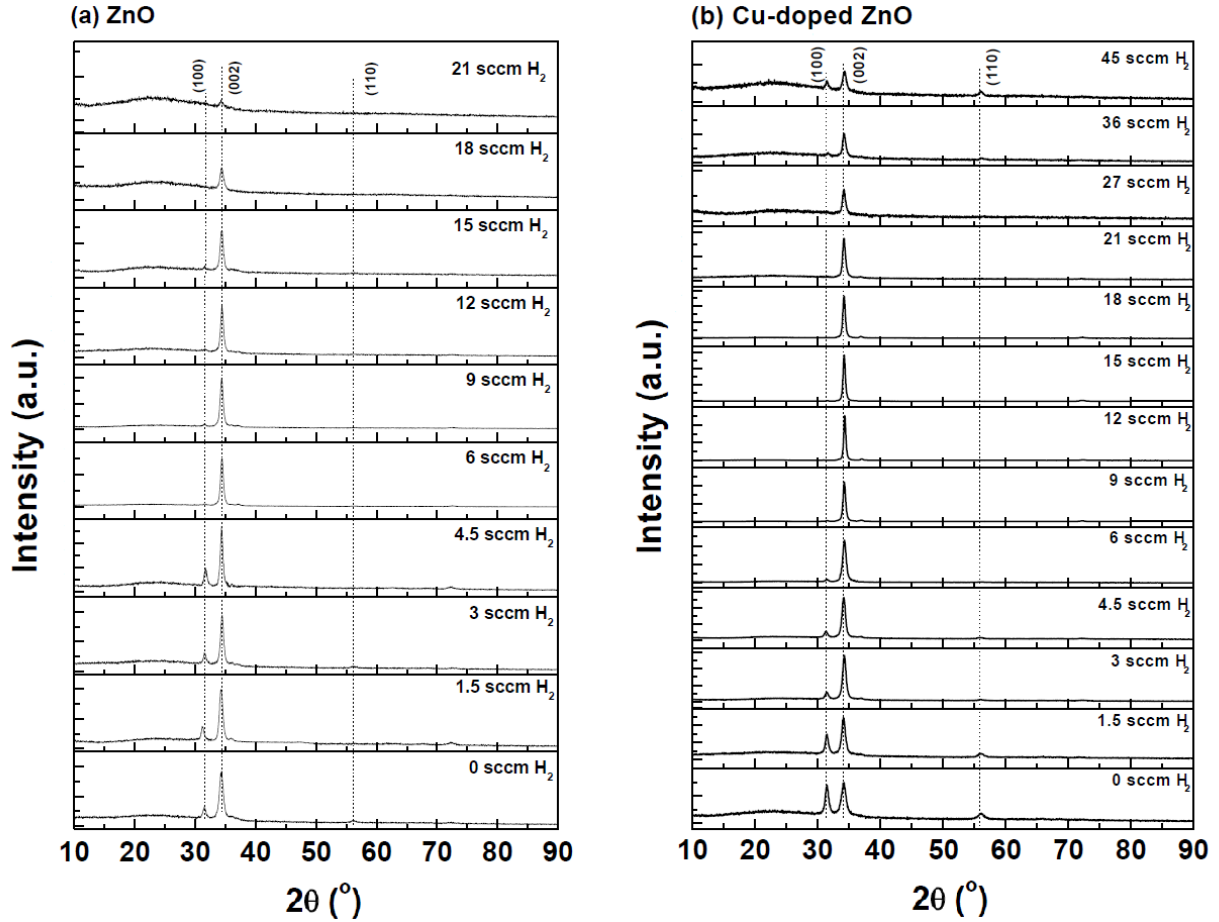


Figure 2. XRD patterns of the ZnO (a) and Cu-doped ZnO (b) films deposited with different  $H_2$  fluxes

diffraction peaks from (100) and (002) planes. As the  $H_2$  flux increases, the (100) diffraction peak of the films gradually weakens and at  $H_2$  flux above 6 sccm (except for the films prepared at  $H_2$  flux of 36 and 45 sccm) the films only exhibit diffraction peak from (002) plane. The (002) diffraction peak intensity of the films shows a trend of first increasing and then decreasing with the increase of  $H_2$  flux, but their intensity is significantly higher than that of the ZnO films. To quantify the preferred orientation, the coefficient of texture ( $TC$ ) of the films can be calculated by the following formula [31]:

$$TC_{(h_i k_i l_i)} = \frac{I(h_i k_i l_i)}{I_0(h_i k_i l_i)} \left[ \frac{1}{n} \sum_{i=1}^n \frac{I(h_i k_i l_i)}{I_0(h_i k_i l_i)} \right]^{-1} \quad (1)$$

where  $I(h_i k_i l_i)$  and  $I_0(h_i k_i l_i)$  are the intensities of  $(h_i k_i l_i)$  diffraction peaks of the film and the standard powder sample, respectively. Three diffraction peaks of (100), (002) and (110) are taken into account in this study (namely,  $n = 3$ ). The  $TC_{(100)}$  and  $TC_{(002)}$  of the ZnO and Cu-doped ZnO films as functions of  $H_2$  flux are shown in Fig. 3a. With the increase of  $H_2$  flux,  $TC_{(100)}$  of the ZnO films tends to decrease at first and then slightly increase, and that of the Cu-doped ZnO film shows an obvious decrease at first, followed by no change, and finally an obvious increase. For both films, the changed

trend of  $TC_{(002)}$  is exactly opposite to that of  $TC_{(100)}$  with increasing  $H_2$  flux. The changed trends with increase of  $H_2$  flux of  $TC_{(100)}$  and  $TC_{(002)}$  are consistent with those of intensity of diffraction peaks from (100) and (002) planes. In summary, the above results indicate that introducing an appropriate amount of  $H_2$  during sputtering can achieve high  $TC_{(002)}$ , that is, improve (002) preferred orientation of the films. But excessive  $H_2$  flux can lead to the decrease of  $TC_{(002)}$ , namely, degrade (002) preferred orientation. Overall, regardless ZnO or Cu-doped ZnO films,  $TC_{(002)}$  is greater than  $TC_{(100)}$ , indicating that the films generally exhibit (002) preferred orientation.

In order to further analyse the influence of  $H_2$  flux on the structure of the ZnO and Cu-doped ZnO films, Fig. 3b shows the position of (002) diffraction peak [ $2\theta_{(002)}$ ] and its full width at half maximum [ $FWHM_{(002)}$ ] as functions of  $H_2$  flux. As it can be seen, the  $2\theta_{(002)}$  value of the ZnO and Cu-doped ZnO films tends to increase at first and then decrease with the increase of  $H_2$  flux. At the same  $H_2$  flux, the  $2\theta_{(002)}$  value of the Cu-doped ZnO films is smaller than that of the ZnO films. For the  $FWHM_{(002)}$  of the ZnO and Cu-doped ZnO films, it first decreases and then increases with the increase of  $H_2$  flux. Based on  $2\theta_{(002)}$  and  $FWHM_{(002)}$ , the crystallite size ( $D$ ) of the films is calculated by the Scherrer formula [32], and the results are also shown in Fig.

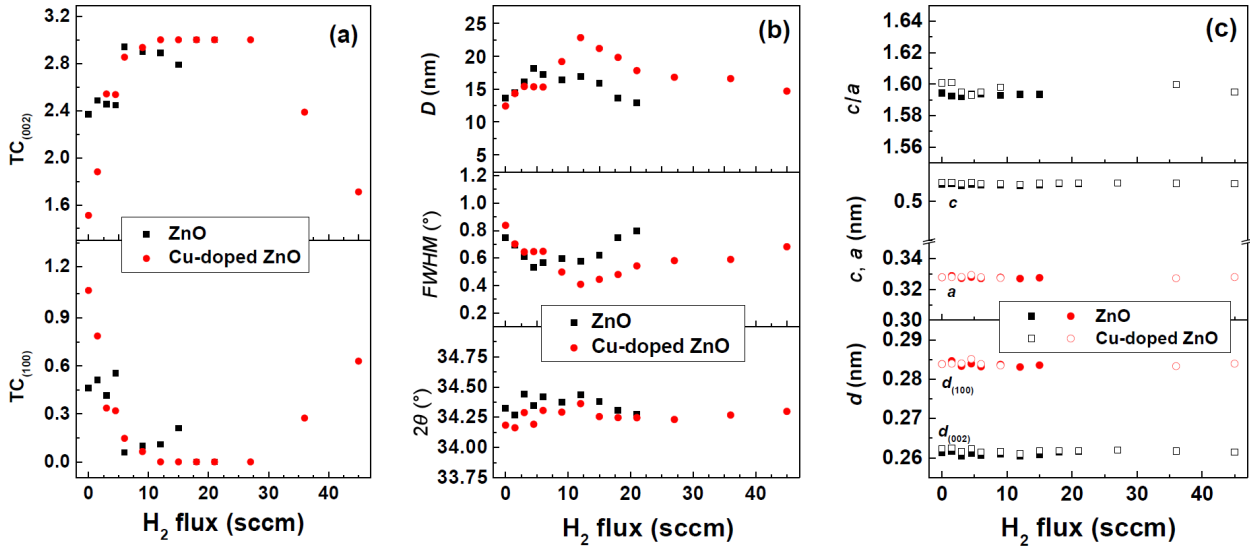


**Figure 3. Structural characteristics of the ZnO and Cu-doped ZnO films as functions of H<sub>2</sub> flux: a)  $TC_{(100)}$  and  $TC_{(002)}$ , b)  $2\theta$  value and FWHM of (002) diffraction peak as well as crystallite size ( $D$ ) and c) lattice parameters ( $c$ ,  $a$ ,  $c/a$ ) and  $d$ -space ( $d_{(100)}$  and  $d_{(002)}$ )**

3b. As it is expected, the crystallite size of the film is inversely proportional to the FWHM of the diffraction peak. Therefore, the crystallite size tends to first increase and then decrease. This result is different from the previously reported crystallite size of ZnO or Cu-doped ZnO films, which remained basically unchanged or decreased with increasing H<sub>2</sub> flux [26,27].

In addition to  $FWHM_{(002)}$  and  $2\theta_{(002)}$ , the lattice parameters  $c$  and  $a$  of the films can be calculated through formulas  $c = \lambda / \sin \theta_{(002)}$  and  $a = \lambda / \sqrt{3} \sin \theta_{(100)}$  ( $\lambda$  is the wavelength of Cu K $\alpha_1$  radiation and  $\theta$  is the Bragg angle), respectively. The interplanar spacing  $d_{(002)}$  and  $d_{(100)}$  of the films can be calculated according to the Bragg equation  $d = \lambda / 2 \sin \theta$ . The lattice parameters ( $c$ ,  $a$  and  $c/a$ ) and  $d$  ( $d_{(100)}$  and  $d_{(002)}$ ) of the ZnO and Cu-doped ZnO films as functions of H<sub>2</sub> flux are shown in Fig. 3c. It should be noted that no (100) diffraction peak was detected in some samples (18–21 sccm H<sub>2</sub> for ZnO films and 12–27 sccm H<sub>2</sub> for Cu-doped ZnO films), and therefore their  $a$ ,  $c/a$  and  $d_{(100)}$  values are not given. With increase of H<sub>2</sub> flux, it can be observed that the lattice parameters and  $d$  had only minor changes. Compared with the standard sample of ZnO powder ( $c = 0.5207$  nm,  $a = 0.3249$  nm and  $c/a = 1.6020$ ), both films have higher  $c$  and  $a$  values but lower  $c/a$  values ( $c = 0.5208$ – $0.5233$  and  $0.5220$ – $0.5249$  nm,  $a = 0.3269$ – $0.3287$  and  $0.3271$ – $0.3293$  nm and  $c/a = 1.5921$ – $1.5944$  and  $1.5931$ – $1.6011$  for the ZnO and Cu-doped ZnO films, respectively). Similarly, both films have larger  $d_{(100)}$  and  $d_{(002)}$  values than those of standard powder sample. The changes in these lattice parameters and  $d$  spacing are related to the doping of foreign impurities and native defects in the film. However, there is no significant change in lattice parameters and  $d$  spacing compared to the standard powder sample, indicating that the films maintain the crystal structure of wurtzite.

Compared with the ZnO films, the  $c$  and  $d_{(002)}$  values of the Cu-doped ZnO films are slightly larger, which also indicate that the Cu-doped ZnO films bear slightly larger compressive stress.

The ZnO and Cu-doped ZnO films deposited at lower H<sub>2</sub> fluxes have two diffraction peaks from (100) and (002) planes. This result can be attributed to low substrate temperature and high deposition rate, in which cases adatoms have no sufficient energy and the surface mobility to settle in stable positions [33,34]. Thus, in recent reports, it was mentioned that 0.5 at.% Cu-doped ZnO films deposited at 150 °C exhibited (100) and (002) diffraction peaks, while ZnO or Cu-doped ZnO films deposited at 300 °C only exhibited (002) diffraction peak [26,27]. With the increase of H<sub>2</sub> flux, the amount of active hydrogen species in the sputtering atmosphere increases. These active hydrogen species will eliminate the metastable (100) crystal plane [35], so that the (002) preferred orientation of the film is enhanced. As discussed above, the amount of active hydrogen species in sputtering atmosphere increases with the increase of H<sub>2</sub> flux, and these active hydrogen species will also eliminate the weakly connected atomic clusters on the film surface [36,37], resulting in the increase of crystallite size of the film. However, when the H<sub>2</sub> flux continues to increase, a large amount of active hydrogen species will cause serious corrosion of a crystallite and increase defects in the film, resulting in the decrease of crystallite size of the film. The incorporation of Cu into the ZnO lattice will cause lattice distortion, resulting in the decrease of film crystallinity and crystallite size. However, when the H<sub>2</sub> flux exceeds 6 sccm, the thickness of the Cu-doped ZnO film is significantly larger than that of the ZnO film as mentioned above. This implies that Cu doping slows down the etching effect of hydrogen plasma, so the crystallinity of the Cu-doped ZnO films

is higher and their crystallite size is larger at  $H_2$  flux above 6 sccm.

As mentioned above, hydrogen is inevitably doped into ZnO lattice to form interstitial hydrogen ( $H_i$ ) when ZnO or Cu-doped ZnO films are deposited in  $H_2$ -containing atmosphere, which will increase spacing of (002) crystal plane and thus decrease  $2\theta_{(002)}$  value [12,14,28–30]. However, active hydrogen species and ZnO may undergo redox reaction to produce oxygen vacancy ( $V_O$ ) in the film at the same time [38–40], and hydrogen can also enter the  $V_O$  position to form substitutional hydrogen ( $H_O$ ) [13]. The formation of defects  $V_O$  and/or  $H_O$  will lead to the increase of  $2\theta_{(002)}$ . When the  $H_2$  flux increases from 0 to 12 sccm, the  $2\theta_{(002)}$  of ZnO film tends to increase, which means that the increase in number of  $V_O$  and  $H_O$  defects is larger than that of  $H_i$  defects in the films. On the contrary, as the  $H_2$  flux increases from 12 to 21 sccm, a decreasing trend in  $2\theta_{(002)}$  of ZnO films may be due to the fact that the increase in the number of  $H_i$  defects is larger than that of  $V_O$  and  $H_O$  defects in the films. For the Cu-doped ZnO films, the change trend of  $2\theta_{(002)}$  with increasing  $H_2$  flux from 0 to 21 sccm is similar to that of the ZnO films, but the corresponding  $2\theta_{(002)}$  values are smaller. The smaller  $2\theta_{(002)}$  values of the Cu-doped ZnO films should be related to the incorporation of Cu into the ZnO lattice. In ZnO lattice, Cu ions may exist in two states:  $Cu^+$  and  $Cu^{2+}$ . According to the relevant reports [41], the radii of  $Cu^+$ ,  $Cu^{2+}$  and  $Zn^{2+}$  are 0.096, 0.072 and 0.074 nm respectively. When  $Cu^+$  replaces  $Zn^{2+}$  or when  $Cu^{2+}$  is located in the lattice interstitial sites, the spacing of the (002) crystal plane increases. Thus, the  $2\theta_{(002)}$  values of the Cu-doped ZnO films are smaller than those of the ZnO films in the  $H_2$  flux range of 0–21 sccm. When the  $H_2$  flux increases from 21 to 45 sccm, the  $2\theta_{(002)}$  of the Cu-doped ZnO film remains basically unchanged, which may be due to the various defects in the film reaching equilibrium. Compared with  $2\theta_{(002)}$  of the ZnO standard sample ( $34.42^\circ$ ),  $2\theta_{(002)}$  of all the films is basically lower, indicating the presence of compressive stress in the films.

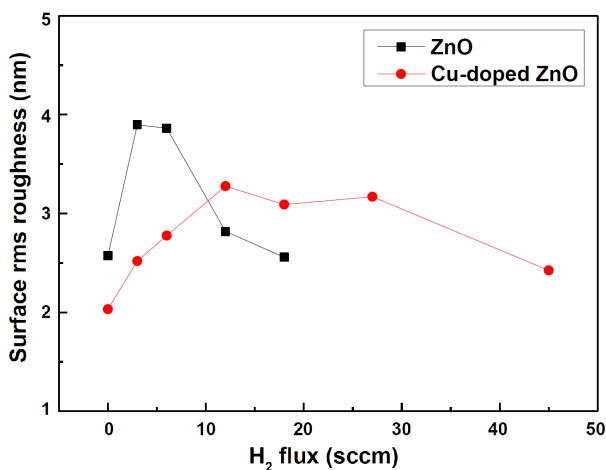


Figure 4. The surface root mean square (RMS) roughness of ZnO and Cu-doped ZnO films as a function of  $H_2$  flux

As the  $H_2$  flux increases,  $2\theta_{(002)}$  shows a trend of first increasing and then decreasing, which means that the compressive stress of the films tends to first decrease and then increase. The  $2\theta_{(002)}$  values of the Cu-doped ZnO films are smaller than those of ZnO films, which indicates smaller compressive stress in the Cu-doped ZnO films.

Figure 4 presents the variation of the surface root mean square (RMS) roughness of the films with  $H_2$  flux. With the increase of  $H_2$  flux, it can be seen that the roughness of both ZnO and Cu-doped ZnO films increases at first and then decreases. Compared with the ZnO film, the surface roughness of the Cu-doped ZnO film is smaller at  $H_2$  flux of 0–6 sccm but larger at  $H_2$  flux greater than 6 sccm. As discussed above, the hydrogen plasma is formed during sputtering after the introduction of  $H_2$ . Obviously, the etching effect of the hydrogen plasma will enlarge and deepen the boundary between the particles on the film surface, thereby increasing the surface roughness. However, when the  $H_2$  flux is too high, the stronger etching effect of hydrogen plasma will reduce the particle size. As a result, the film thickness and surface roughness decrease. The relationship between the film thickness and  $H_2$  flux has indicated that the ZnO films are easier to be etched by hydrogen plasma than the Cu-doped ZnO films, so the surface roughness of the ZnO films is larger than that of the Cu-doped ZnO films at  $H_2$  flux of 0–6 sccm. When the  $H_2$  flux is greater than 6 sccm, the further etching results in refinement of particles and significant reduction in thickness of the ZnO film, so its surface roughness is lower than that of the Cu-doped ZnO film.

Cross-sectional SEM images of the representative ZnO and Cu-doped ZnO films are shown in Fig. 5. It can be observed that the cross-sectional morphology of the films is a columnar structure. This columnar morphology has also been observed in previous studies [6,9,29,30], and it is consistent with the result of the film having (002) preferred orientation. In addition, the thickness of the films obtained from cross-sectional images is basically consistent with that measured by interference microscopy.

The wide-scan XPS spectra of the films indicate that, except for C contamination, only Zn and O elements are present in the ZnO films and only Cu, Zn and O elements are present in the Cu-doped ZnO films. In order to further analyse the chemical state of elements in the films, Fig. 6 gives high-resolution XPS spectra of O 1s and Cu  $2p_{3/2}$  as well as Auger spectra of Zn  $L_{3M_{45}M_{45}}$  for the ZnO and Cu-doped ZnO films. As shown in Figs. 6a and 6b, the XPS spectra of O 1s can be decomposed into three sub-peaks, and these three sub-peaks centre at about 530, 531 and 532 eV, respectively. The sub-peak centred at about 532 eV is related to oxygen species that are chemisorbed and weakly bonded or adsorbed at film surface such as  $-CO_3$ ,  $-OH$ ,  $H_2O$  or  $O_2$  [29,38,40]. Other two sub-peaks centred at about 530 and 531 eV can be attributed to  $O^{2-}$  in the normal ZnO lattice and

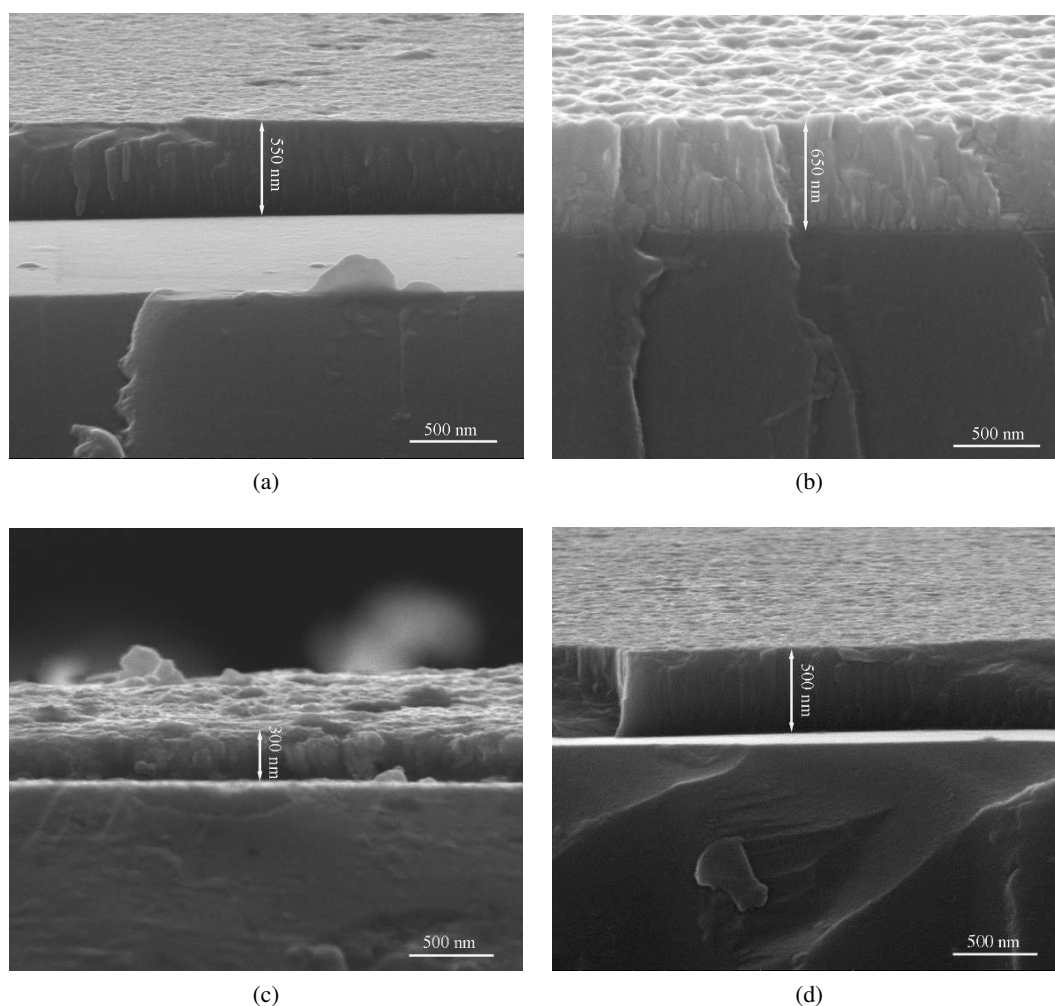


**Figure 5. Cross-sectional SEM images of ZnO-based films: a) ZnO, 0 sccm H<sub>2</sub>, b) Cu-doped ZnO, 0 sccm H<sub>2</sub>, c) ZnO, 9 sccm H<sub>2</sub> and d) Cu-doped ZnO, 9 sccm H<sub>2</sub>**

O<sup>2-</sup> in the oxygen deficient region in ZnO lattice, respectively [29,38,40], and thus their area ratio can be utilized to evaluate the  $V_O$  content in the films. From the area ratios shown in Figs. 6a and 6b, it can be found that the  $V_O$  content in the ZnO film shows a trend of first decreasing and then increasing, while the  $V_O$  content in the Cu-doped ZnO film shows a decreasing trend with the increase of H<sub>2</sub> flux. At the same H<sub>2</sub> flux, the  $V_O$  content in the Cu-doped ZnO films is lower than that of the ZnO films. Because the XPS spectra of Zn 2p<sub>3/2</sub> and Zn 2p<sub>1/2</sub> show high symmetry and the difference between the binding energies of Zn<sup>0+</sup> and Zn<sup>2+</sup> is small, it is not easy to analyse the chemical state of Zn in the film by peak deconvolution of XPS spectra of Zn 2p<sub>3/2</sub> or Zn 2p<sub>1/2</sub> [42,43]. Figures 6c and 6d give the Auger spectra of Zn L<sub>3</sub>M<sub>45</sub>M<sub>45</sub> in order to analyse the chemical state of Zn in the films. It can be observed that the Auger spectra of Zn L<sub>3</sub>M<sub>45</sub>M<sub>45</sub> have a main peak and an obvious shoulder peak. These two peaks are located at about 498 and 495 eV, and they are correspond to the binding energies of Zn<sup>2+</sup> and metallic Zn (i.e. interstitial zinc, Zn<sub>i</sub>), respectively. The area ratio of the shoulder peak to the main peak is utilized to estimate Zn<sub>i</sub> content in the films. It can be seen that Zn<sub>i</sub> content of both

ZnO and Cu-doped ZnO films increases at first and then decreases with the increase of H<sub>2</sub> flux. Compared with the Cu-doped ZnO films, Zn<sub>i</sub> content in ZnO films is larger at H<sub>2</sub> flux of 0 and 6 sccm, but it is smaller at H<sub>2</sub> flux of 18 sccm. The XPS spectra of Cu 2p<sub>3/2</sub> of the Cu-doped ZnO film are shown in Fig. 6e. Based on the reported binding energies of Cu with different valence states [44], the spectra are decomposed. From the area ratio of decomposed peaks, the Cu<sup>+</sup>/Cu<sup>2+</sup> ratio in the film gradually increases as the H<sub>2</sub> flux increases from 0 to 18 sccm. At H<sub>2</sub> flux of 45 sccm, Cu<sup>2+</sup> disappears and Cu appears in the film. In addition, according to the area of Cu 2p<sub>3/2</sub> and Zn 2p<sub>3/2</sub> peaks and the element sensitivity factor, the atomic ratios of Cu/Zn in the films are 0.024, 0.023, 0.032 and 0.036 when the H<sub>2</sub> flux is 0, 6, 18 and 45 sccm, respectively.

The following redox reaction should exist between active hydrogen species (H\*) and ZnO: ZnO + 2H\* → Zn + H<sub>2</sub>O. Thus, it is clear that the introduction of H<sub>2</sub> into deposition atmosphere may increase  $V_O$  and/or Zn<sub>i</sub> defects in the films. But the hydrogen implanted in the film can enter  $V_O$  site to form H<sub>O</sub> as mentioned above, thereby reducing  $V_O$  content in the films. In the current study,  $V_O$  content of the ZnO films shows a trend of first

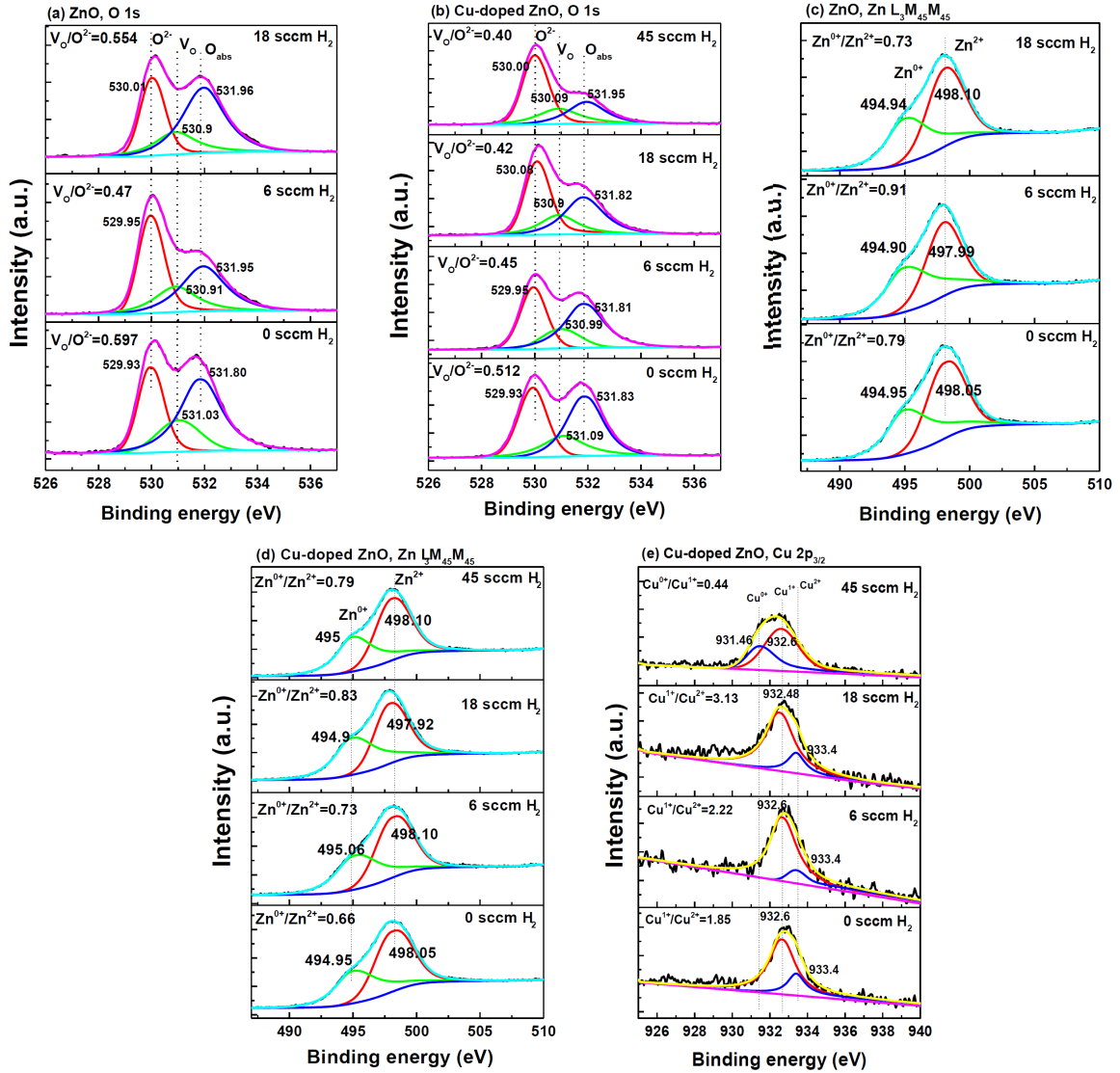


Figure 6. High-resolution XPS spectra of O 1s (a, b), Auger spectra of Zn L<sub>3</sub>M<sub>45</sub>M<sub>45</sub> (c, d) and XPS spectra of Cu 2p<sub>3/2</sub> (e) of the ZnO (a, c) and Cu-doped ZnO (b, d, e) films deposited at different H<sub>2</sub> fluxes

decreasing and then increasing, which indicates that the passivation of V<sub>O</sub> by hydrogen is dominant when a small amount of H<sub>2</sub> is introduced, while redox reaction plays a major role when excess H<sub>2</sub> is introduced. For the Cu-doped ZnO films, V<sub>O</sub> content decreases with the increase of H<sub>2</sub> flux, indicating that hydrogen plays a dominant role in the passivation of V<sub>O</sub>, while the effect of redox reaction between H\* and ZnO is relatively weaker. Content of Zn<sub>i</sub> in the ZnO and Cu-doped ZnO films firstly increases with the increase of H<sub>2</sub> flux, which is related to the enhanced redox reaction between H\* and ZnO. When the H<sub>2</sub> flux is too high, Zn<sub>i</sub> content in the films decreases. The possible reason is that the following reaction may exist between H<sub>2</sub> and Zn under high flux of H<sub>2</sub>: Zn + H<sub>2</sub> → ZnH<sub>2</sub> ↑ [45]. At the same H<sub>2</sub> flux, it can be seen from the sum of peak area ratios of V<sub>O</sub>/O<sup>2-</sup> and Zn/Zn<sup>2+</sup> that the total content of V<sub>O</sub> and Zn<sub>i</sub> defects in the ZnO film is higher than that of the Cu-doped ZnO film. This indicates that the ZnO film is

easier to be etched, which is consistent with the above analysis results of film thickness and surface roughness. Due to the deoxidation function of H\*, the Cu<sup>+</sup>/Cu<sup>2+</sup> ratio gradually increases with initial increase of H<sub>2</sub> flux, while Cu<sup>2+</sup> disappears and Cu appears with further increase of H<sub>2</sub> flux in the Cu-doped ZnO films. As discussed above, more ZnO is etched by hydrogen plasma as the H<sub>2</sub> flux increases, resulting in an increase in the atomic ratio of Cu/Zn in the films.

### 3.2. Electrical properties

Figure 7 presents the electrical properties of the ZnO and Cu-doped ZnO films as functions of H<sub>2</sub> flux. The resistivity of the ZnO film is 4.43 Ω·cm at H<sub>2</sub> flux of 0 sccm, while that of the Cu-doped ZnO cannot be measured at H<sub>2</sub> flux of 0–3 sccm due to high resistivity. With the increase of H<sub>2</sub> flux, the resistivity of the ZnO films first decreases and then increases, while that of the Cu-doped ZnO films continues to decrease. For the ZnO

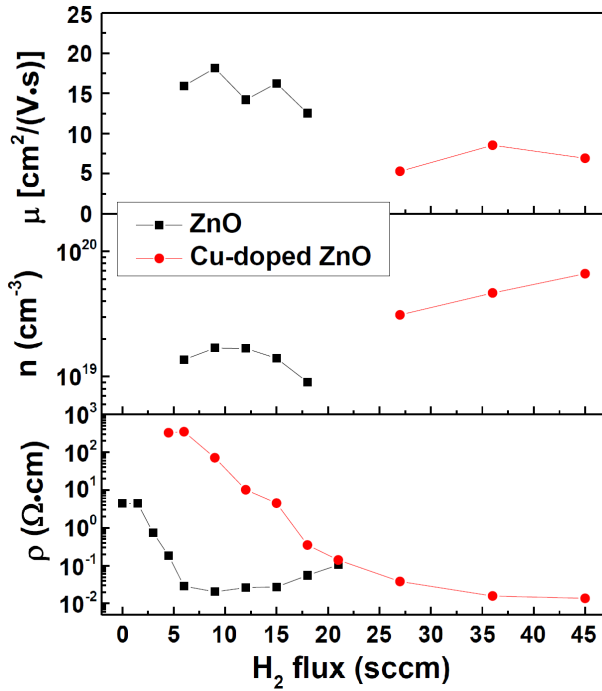


Figure 7. The resistivity ( $\rho$ ), carrier concentration ( $n$ ) and Hall mobility ( $\mu$ ) of the ZnO and Cu-doped ZnO films as functions of  $H_2$  flux

films, the resistivity decreases to about  $2.5 \times 10^{-2} \Omega\cdot\text{cm}$  at  $H_2$  flux of 6–15 sccm, and then increases to  $1.05 \times 10^{-1} \Omega\cdot\text{cm}$  at  $H_2$  flux of 21 sccm. For the Cu-doped ZnO films, the resistivity is  $3.23 \times 10^2 \Omega\cdot\text{cm}$  at  $H_2$  flux of 4.5 sccm, and then it drops to  $1.37 \times 10^{-2} \Omega\cdot\text{cm}$  as the  $H_2$  flux increases to 45 sccm. This low resistivity ( $1.37 \times 10^{-2} \Omega\cdot\text{cm}$ ) is higher than that reported by Zhou *et al.* ( $6.67 \times 10^{-3} \Omega\cdot\text{cm}$ ) [23], but much lower than those obtained by Cai *et al.* ( $1.90 \times 10^2 \Omega\cdot\text{cm}$ ) [25] and reported previously by our group ( $67.54 \Omega\cdot\text{cm}$ ) [26]. Moreover, it is lower than the low resistivity ( $2.5 \times 10^{-2} \Omega\cdot\text{cm}$ ) obtained from hydrogen-doped ZnO films in this study. In general, the ZnO and Cu-doped ZnO films with resistivity lower than  $10^{-1} \Omega\cdot\text{cm}$  can be obtained when the  $H_2$  flux ranges from 6 to 18 sccm and from 27 to 45 sccm, respectively. For the films prepared in these two  $H_2$  flux ranges, the carrier concentration and Hall mobility can be accurately measured due to their low resistivity. Comparing the carrier concentration and mobility of the ZnO and Cu-doped ZnO films prepared in these two  $H_2$  flux ranges, the ZnO films have lower carrier concentration but higher mobility.

As mentioned above, Cu can act as an acceptor impurity after doping into ZnO films, and thus *p*-type ZnO films can be obtained [8,9]. Under pure Ar atmosphere (0 sccm  $H_2$ ), the resistivity of the Cu-doped ZnO film is significantly higher than that of the ZnO film, which can be attributed to Cu acting as an acceptor impurity to reduce free electrons in ZnO films. When the ZnO or Cu-doped ZnO films are deposited under Ar +  $H_2$  atmosphere, the decrease of film resistivity is related to hydrogen doping into ZnO to form  $H_i$  and  $H_O$  donor

impurities [12,13], the deoxidation of ZnO by hydrogen plasma to increase  $V_O$  and  $Zn_i$  donor defects [17,38–40,46] and hydrogen passivating acceptor defects such as zinc vacancy ( $V_{Zn}$ ) [29,36]. When Cu is present in the films, to obtain lower resistivity, more donor impurities or defects need to be generated in the film to compensate for the decrease in electron concentration caused by Cu doping. Therefore, the range of  $H_2$  flux in which lower resistivity is obtained shifts to larger  $H_2$  fluxes for the Cu-doped ZnO films. For the ZnO films, the film resistivity increases as the  $H_2$  flux increases from 15 to 21 sccm, which can be ascribed to the decrease in crystallinity [35]. The Cu-doped ZnO films have higher carrier concentration than the ZnO films, which may be related to the larger flux of  $H_2$  introduced and the higher film crystallinity. Due to the incorporation of Cu, the impurity scattering in the film increases significantly, so the charge carrier mobility of the Cu-doped ZnO films is lower than that of the ZnO films.

In order to investigate the electrically conductive stability, the ZnO and Cu-doped ZnO films with resistivity lower than  $10^{-1} \Omega\cdot\text{cm}$  were exposed to air, and the film resistivity was tested continuously at certain time interval for one month. The ratio of resistivity obtained after exposure in air to the initial resistivity is plotted as a function of exposure time in air, as shown in Fig. 8. In general, the resistivity of most films increases rapidly after exposure to air for 4–7 days, and then the resistivity basically shows a trend of slow increase or gradual stabilization as the exposure time in air is further prolonged. After the ZnO films are exposed to air for 30

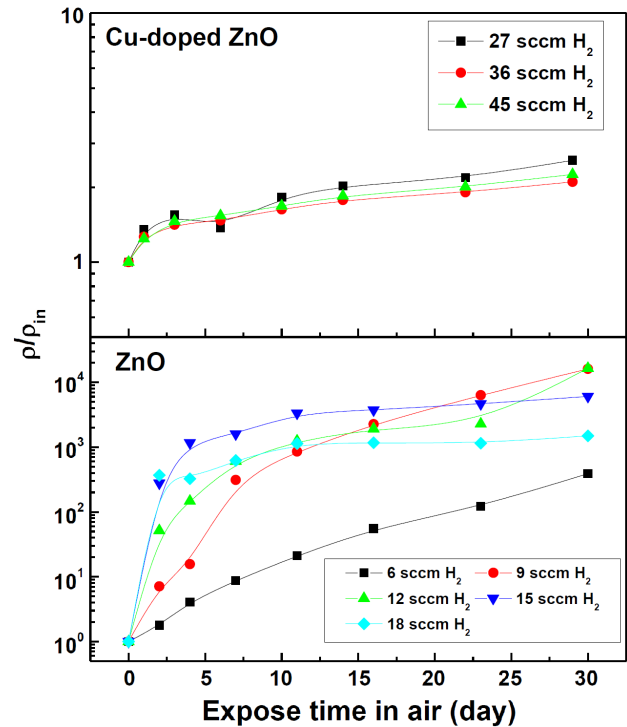


Figure 8. The ratio of resistivity obtained after exposure in air to the initial resistivity ( $\rho/\rho_{in}$ ) of typical films as a function of exposure time in air

days, the resistivity of the film prepared at  $H_2$  flux of 6 sccm increases by about  $10^2$  times, while that of the films prepared at  $H_2$  flux of 12–18 sccm increases by about  $10^3$ – $10^4$  times. As mentioned above, the resistivity of the ZnO film can drop to the order of magnitude of  $10^{-2} \Omega\cdot\text{cm}$  after the introduction of  $H_2$  during sputtering, but it increases to the order of magnitude  $10^2$ – $10^3 \Omega\cdot\text{cm}$  with the prolonged exposure to air. For the Cu-doped ZnO films prepared at  $H_2$  flux of 27–45 sccm, the resistivity increases by about 2 times after exposure to air for 30 days. In comparison, the resistivity of previously reported 0.5 at.% Cu doped-ZnO films significantly increased after 30 days of exposure to air (30–60 times at 150 °C and 8–10 times at 300 °C) [27]. It is clear that the Cu-doped ZnO film can not only obtain low resistivity in a suitable range of  $H_2$  flux, but also maintain low resistivity even if the film is exposed to air for a long time as in this study.

When ZnO or Cu-doped ZnO films are exposed to air,  $O_2$  and/or  $H_2O$  in the air will gradually be adsorbed on grain boundaries of the films, and these adsorbed  $O_2$  and/or  $H_2O$  will capture electrons and form grain boundary barriers to hinder electron transport [47,48]. As a result, the film resistivity increases after exposure to air. Obviously, the increase in the film resistivity is related to the amount of adsorbed  $O_2$  and/or  $H_2O$ . Furthermore, the amount of adsorbed  $O_2$  and/or  $H_2O$  depends on the microstructure and lattice defects of the film. From XRD and XPS results, the crystallite size of the ZnO film decreases and its  $V_O$  content increases as the  $H_2$  flow rate increases from 6 to 18 sccm. These changes in microstructure and lattice defects are beneficial to the adsorption of  $O_2$  and/or  $H_2O$  from air by the ZnO films. In addition, it is particularly worth noting that the hydrogen incorporation into the ZnO film is mainly in the form of  $H_i$ . Although theoretical and experimental studies have shown that this defect is stable at RT [15,49], some researchers have also observed that the formation of  $H_2$  or overflow of  $H_i$  leads to the increase of film resistivity [50,51]. When the films are exposed to air for a period of time, the adsorption of  $O_2$  and/or  $H_2O$  and the overflow of  $H_i$  reach saturation, and thus the resistivity tends to be stable. Compared with ZnO films, electrical conduction stability of the Cu-doped ZnO films significantly improves. The reasons behind this can be attributed to the following several aspects: i) Cu-doped ZnO films can maintain higher crystallinity and thickness even at the  $H_2$  flux of 27–45 sccm; ii) the amount of  $V_O$  generated in the film is relatively smaller, as mentioned above; and iii) it may be easier to form thermally more stable Cu–H and  $H_O$  defects due to the existence of Cu in the film, thus avoiding the overflow of  $H_i$ .

In order to further explore the defect form and stability of hydrogen in the films, the ZnO film prepared at  $H_2$  flux of 9 sccm and the Cu-doped ZnO film prepared at  $H_2$  flux of 36 sccm were underwent vacuum annealing. The ratio of the resistivity obtained after vacuum annealing to the initial resistivity as a function of an-

nealing temperature is shown in Fig. 9. It can be found that the resistivity of the ZnO and Cu-doped ZnO films increases by about  $10^3$  and  $10^4$  times after annealing treatment at 150 °C, respectively. This increase is related to the escape of the thermally less stable  $H_i$  in the film during annealing [15,35,49]. The escape of the  $H_i$  reduces the carrier concentration of the films and thus the resistivity increases. The resistivity of the film decreases slightly as the annealing temperature increases from 150 to 300 °C. This is because the film crystallinity enhances after high temperature treatment on one hand, and more  $V_O$  will be formed in the film under vacuum annealing atmosphere on the other hand [35]. With further increasing of the annealing temperature to 450 °C, the films are obviously darkened to the naked eye. This implies that metal nanoparticles are formed in the films due to the release of a large amount of oxygen at high annealing temperature under vacuum. The formed metal nanoparticles hinder the electron transport, and thus the film resistivity increases again.

After annealing, the resistivity of both ZnO and Cu-doped ZnO films significantly increases, indicating that their thermal stability of electrical properties is poor. What's more, the increase in resistivity of the Cu-doped ZnO film is larger than that of the ZnO film at the same annealing temperature, which means that Cu doping does not enhance the thermal stability of electrical properties of ZnO film. The poor thermal stability of electrical properties for both ZnO and Cu-doped ZnO films implies existence of a large number of  $H_i$  defects with low thermal stability. But as mentioned in Introduction, Cai *et al.* [25] found that the resistivity of Cu and hydrogen co-doped films was not increased after annealing treatment, indicating that the thermal stability of hydrogen-related donors in films was high and the donor with high thermal stability might be Cu–H complex. Between our results and results presented in Cai *et al.* [25], different hydrogen-related defects formed in the film should be related to the different ways in which

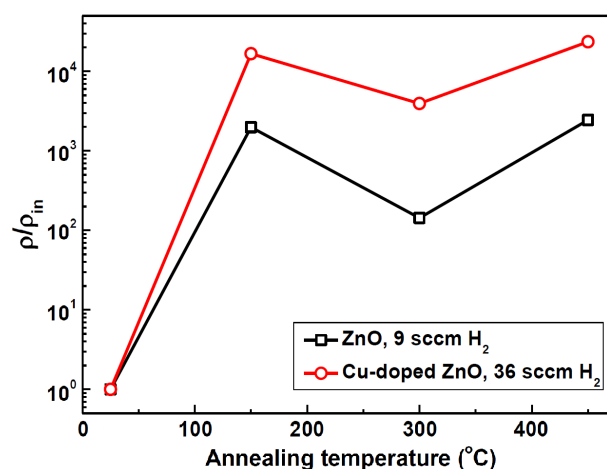


Figure 9. The ratio of resistivity obtained after vacuum annealing to the initial resistivity ( $\rho/\rho_{in}$ ) of typical films as a function of vacuum annealing temperature

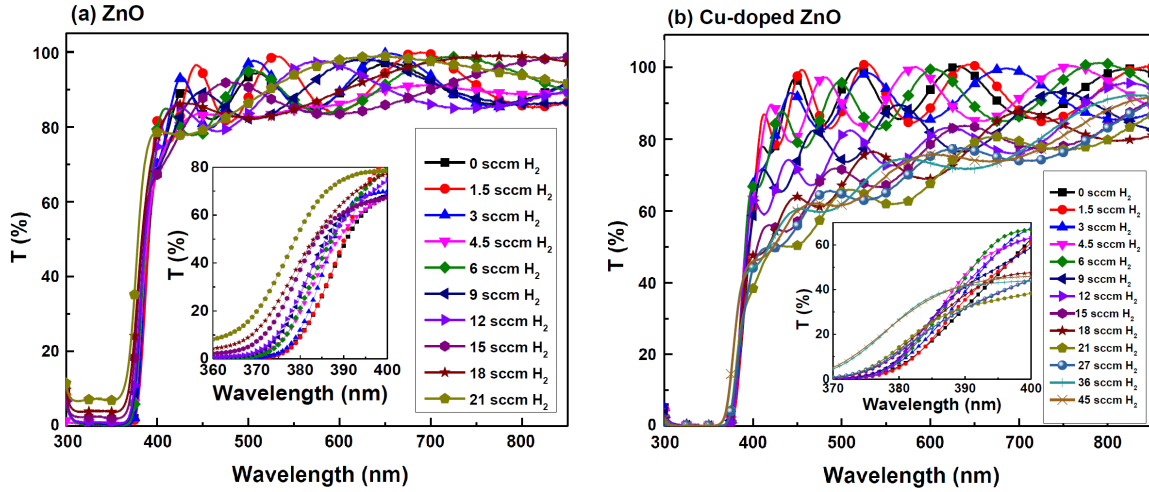


Figure 10. The transmittance spectra of the ZnO (a) and Cu-doped ZnO (b) films deposited with different H<sub>2</sub> fluxes

hydrogen is introduced into the film. After annealing at 150 °C, the resistivities of the ZnO film prepared at H<sub>2</sub> flux of 9 sccm and the Cu-doped ZnO films prepared at H<sub>2</sub> flux of 36 sccm increase to about  $4 \times 10^1$  and  $2.6 \times 10^2 \Omega\cdot\text{cm}$ , which are larger and smaller than those of the ZnO and Cu-doped ZnO films prepared under Ar atmosphere ( $4.43$  and  $> 3.23 \times 10^2 \Omega\cdot\text{cm}$ ), respectively. This indicates that the main defect affecting the resistivity in the ZnO films is H<sub>i</sub> despite the existence of defects such as V<sub>O</sub> or Zn<sub>i</sub> in the film. However, in the Cu-doped ZnO films, a certain number of defects such as H<sub>O</sub> and Cu–H with high thermal stability should remained although the overflow of H<sub>i</sub> leads to a significant increase in resistivity [15,21,49].

### 3.3. Optical properties

Figure 10 shows the transmittance spectra of the ZnO and Cu-doped ZnO films prepared at different H<sub>2</sub> fluxes. The transmittance spectra show wavy-shape in the visible light range (400–800 nm), which is caused by the interference of the incident light at the film-air and film-substrate interfaces. The average transmittance in the visible light range ( $T_{Vis}$ ) of the films as a func-

tion of H<sub>2</sub> flux is shown in Fig. 11a. With the increase of H<sub>2</sub> flux,  $T_{Vis}$  of the ZnO film changes irregularly around 90%, whereas for the Cu-doped ZnO films it is around 90% at the H<sub>2</sub> flux of 0–6 sccm, but it gradually decreases to about 70% with further increase of H<sub>2</sub> flux to 21 sccm. Generally,  $T_{Vis}$  is related to the crystallinity, thickness, defects and surface roughness of the films [7,18,24,33,39,40]. The improvement of film crystallinity means increase of grain size and decrease of grain boundary density. As the grain boundary density of films decreases, the absorption and scattering of light by the boundaries decrease, resulting in an increase in  $T_{Vis}$ . When there are defects (such as Cu<sub>Zn</sub>, V<sub>O</sub> and Zn<sub>i</sub>) in the films, these defects become centres of light scattering. At the same time, these defects form donor or acceptor energy levels in the bandgap, increasing the absorption of visible light. Thus, the increase of defect amount in the film will reduce  $T_{Vis}$  of the film. As the surface roughness of film increases, the scattering of visible light on the surface increases, resulting in a decrease in  $T_{Vis}$ . A decrease in film thickness will reduce the absorption of visible light, and thus  $T_{Vis}$  increases. In the current study, the grain size of the ZnO films shows a

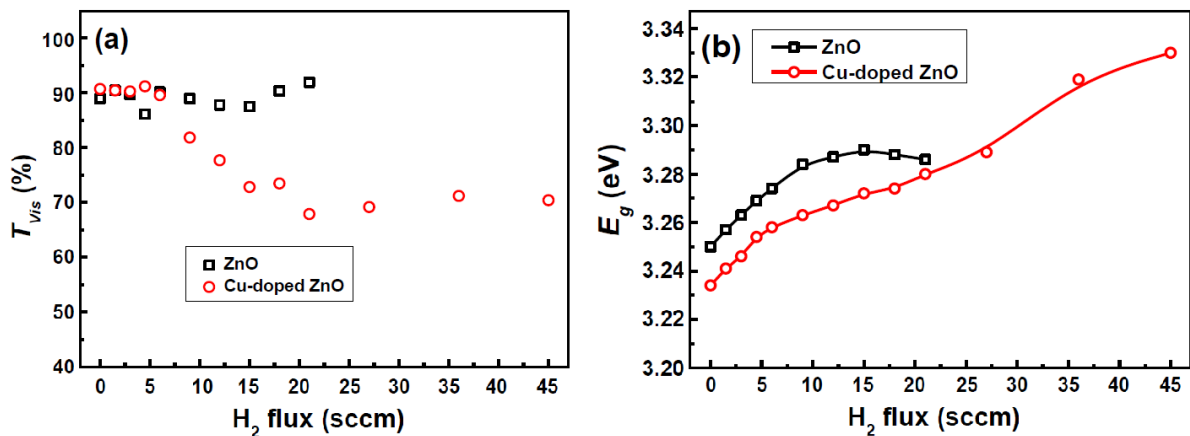


Figure 11. The average transmittance in visible light range ( $T_{Vis}$ ) (a) and band gap ( $E_g$ ) (b) of the ZnO and Cu-doped ZnO films as functions of H<sub>2</sub> flux

trend of first increasing and then decreasing, that is, the grain boundary density in the films first decreases and then increases with the increase of  $H_2$  flux. Meanwhile, the surface roughness of the ZnO films first increases and then decreases. The effects of these two factors on  $T_{vis}$  may mutually offset. As the  $H_2$  flux increases, the number of defects in the ZnO film increases, and thus  $T_{vis}$  of the films will be decreased. However, at the same time, the film thickness decreases obviously for the ZnO films, which will increase  $T_{vis}$ . Taking into account the effects of the above factors, it is not difficult to understand that  $T_{vis}$  of the ZnO films remains basically unchanged, i.e. keeping higher values in the whole  $H_2$  flux range. For the Cu-doped ZnO films, the grain boundary density, surface roughness, defect amount and film thickness as functions of  $H_2$  flux are basically similar to those of the ZnO films. However, it should be noted that the Cu-doped ZnO film is thicker in the whole  $H_2$  flux range. At the same time, according to the analysis results of XPS, the  $Zn_i$  content and atomic ratio of Cu/Zn in the film increase obviously as the  $H_2$  flux increases from 6 to 18 or 45 sccm. In the case of thicker film, the increase of  $Zn_i$  and Cu contents in the film leads to the obvious decrease of  $T_{vis}$  when the  $H_2$  flux increases to 21 sccm.

From the enlarged view of the absorption edge region of the films given in the inset of Fig. 10, the optical absorption edge of the films is basically around 375 nm, and it tends to move towards short-wavelength direction (i.e. blue shift) with the increase of  $H_2$  flux. The shift of the absorption edge reflects the change in  $E_g$  of the film. In order to obtain  $E_g$  value, firstly, the absorption coefficient ( $\alpha$ ) of the film was obtained according to  $T = \exp(-\alpha t)$  ( $T$  is the film transmittance and  $t$  is the film thickness), and then the  $(\alpha hv)^2 \propto hv$  curve is plotted based on Tauc formula  $(\alpha hv)^2 = (hv - E_g)$  ( $hv$  is the photon energy). Finally the linear fit in the absorption edge is extrapolated to intersect the  $hv$  axis [52]. Figure 11b shows  $E_g$  value of the films as a function of  $H_2$  flux. Band gap energy of the ZnO films increases from 3.250 to 3.290 eV when  $H_2$  flux increases from 0 to 15 sccm, and then it slightly decreases to 3.286 eV when  $H_2$  flux further increases to 21 sccm. As the  $H_2$  flux increases from 0 to 45 sccm,  $E_g$  of the Cu-doped ZnO films increases from 3.234 to 3.330 eV. At the same  $H_2$  flux, the  $E_g$  of the ZnO films is larger than that of the Cu-doped ZnO films. It can be found that  $E_g$  of ZnO and Cu-doped ZnO films has the opposite changed trend to their resistivity with the increase of  $H_2$  flux, which reflects the relationship between  $E_g$  of the film and its electrical properties. According to the Burstein-Moss effect,  $E_g$  of the film widens with the increase of the carrier concentration [18,38,52]. Although the carrier concentration of the ZnO and Cu-doped ZnO films prepared at all  $H_2$  fluxes is not given,  $E_g$  of the films is closely related to the Burstein-Moss (BM) effect from above-mentioned relationship between resistivity and  $E_g$ . The strong  $d$ - $p$  coupling of Cu and O leads to the upward shift of the O

$2p$  orbital, and the Cu  $3d$  orbitals create impurity bands above the valence band after the Cu atom enters the Zn site [32,53]. These two effects result in lower  $E_g$  of the Cu-doped ZnO films than ZnO films.

Figures 12a and 12b show the Raman spectra of the ZnO and Cu-doped ZnO films prepared at typical  $H_2$  fluxes, in which the enlarged view of spectra in range of 200–500  $cm^{-1}$  are shown in Figs. 12c and 12d. Raman scattering peaks of the films can be observed at around 100, 135, 185, 275, 330, 380, 440 and 575  $cm^{-1}$ . Among these scattering peaks, those around 100 and 440  $cm^{-1}$  come from the  $E_2^{low}$  and  $E_2^{high}$  vibrational modes, respectively, and the scattering peak around 575  $cm^{-1}$  corresponds to the  $A_1(LO)$  vibrational mode [54]. Generally, the intensity of the scattering peaks of  $E_2$  vibrational modes is related to the film crystallinity, while the intensity of the scattering peaks of  $LO$  vibrational modes is related to the concentration of defects such as  $V_O$ ,  $Zn_i$ , and  $H_i$  in the film [24,37,55–59]. In the current study, the films exhibit weak scattering peaks of  $E_2$  vibrational modes but strong scattering peak of the  $A_1(LO)$  vibrational mode, which indicates that the film crystallinity is poor and there are a lot of defects in the films. The intensity of  $E_2$  scattering peaks of the ZnO and Cu-doped ZnO films shows a trend of increasing first and then weakening, and the maximum intensity is achieved at  $H_2$  flux of 6 and 12 sccm, respectively. Furthermore, the Gaussian-Lorentz mixing function fitting is performed on the  $E_2^{high}$  scattering peak in the range of 390–490  $cm^{-1}$  to obtain FWHM of this scattering peak. As shown in Fig. 12e, FWHM of  $E_2^{high}$  scattering peak of the ZnO and Cu-doped ZnO films tends to first decrease and then increase with the increase of  $H_2$  flux. FWHM of  $E_2^{high}$  scattering peak of the ZnO film is smaller than that of the Cu-doped ZnO film at  $H_2$  flux of 0, 3 and 6 sccm, but the opposite result is observed at  $H_2$  flux of 12 and 18 sccm. It is clear that these results are basically consistent with the change trends of the film crystallinity obtained by XRD. For the scattering peak of the  $A_1(LO)$  vibrational mode of the ZnO and Cu-doped ZnO films, its intensity gradually increases when the  $H_2$  flux increases from 0 to 12 and 27 sccm, respectively, indicating that the sum of  $V_O$ ,  $Zn_i$  and  $H_i$  defects in the films increases. When the  $H_2$  flux increases to 18 and 45 sccm, respectively, the intensity of the  $A_1(LO)$  scattering peak of the ZnO and Cu-doped ZnO films slightly decreases, which may be related to the fact that  $V_O$  and/or  $Zn_i$  decrease somewhat and  $H_i$  content reaches saturation in the films. In addition, as the  $H_2$  flux increases to 18 or 45 sccm, decrease in the intensity of the scattering peak of  $A_1(LO)$  vibrational mode may be related to the decrease in the crystallite size of the films [60]. Although the intensity of both  $E_2^{high}$  and  $A_1(LO)$  scattering peaks tends to increase at first and then decrease, their intensity ratio  $I(A_1(LO))/I(E_2^{high})$  shows increasing trend with increasing  $H_2$  flux, as shown in Fig. 12f. This is because with the increase of  $H_2$  flux, the de-

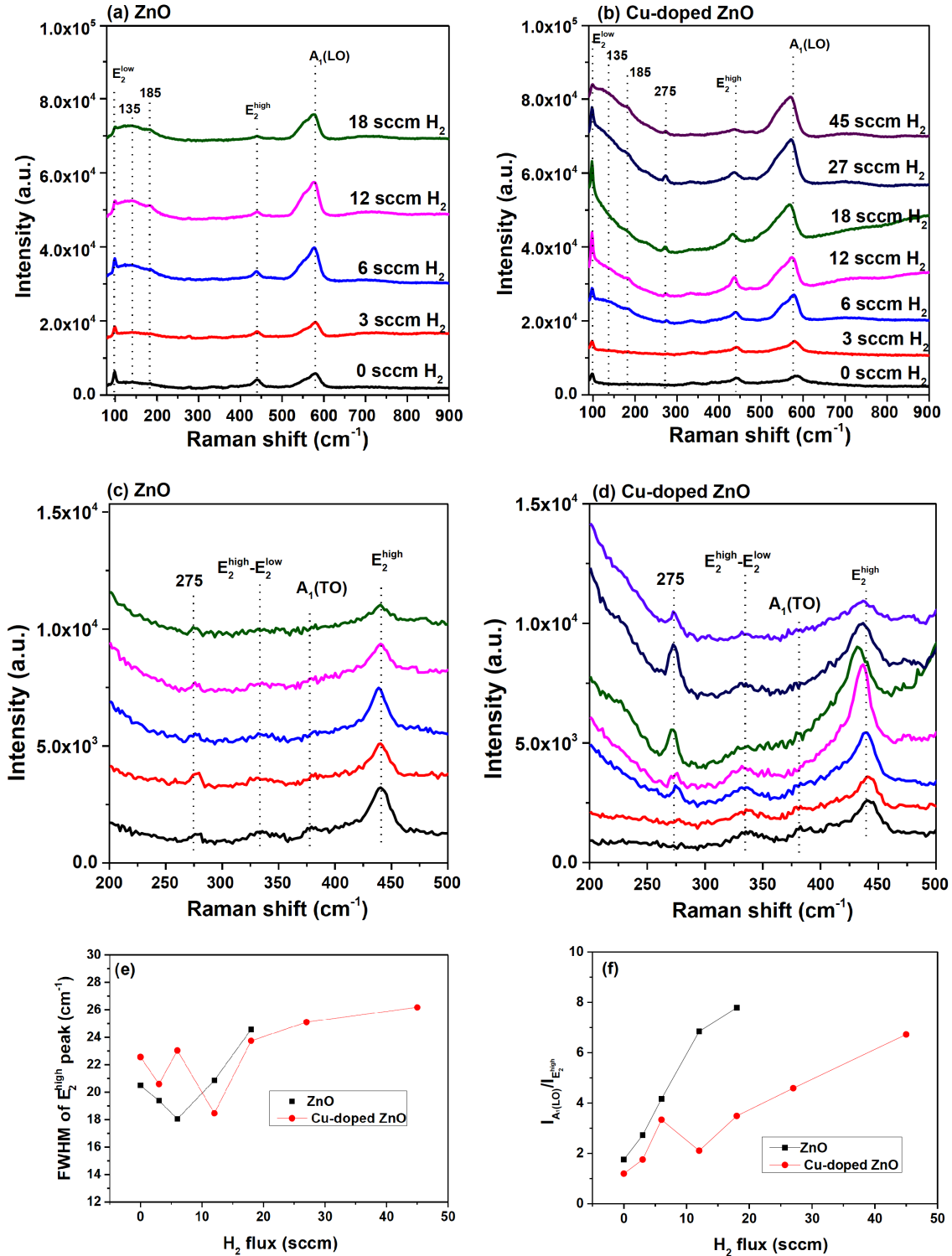


Figure 12. Raman spectra of the ZnO (a, c) and Cu-doped ZnO (b, d) films deposited with different H<sub>2</sub> fluxes in the ranges of 80–900 cm<sup>-1</sup> (a, b) and 200–500 cm<sup>-1</sup> (c, d), and FWHM of E<sub>2</sub><sup>high</sup> (e) and I(A<sub>1</sub>(LO))/I(E<sub>2</sub><sup>high</sup>) (f) as functions of H<sub>2</sub> flux

fects in the films increase more significantly in the lower H<sub>2</sub> flux range, while the film crystallinity degrades more significantly in the higher H<sub>2</sub> flux range. From the Fig. 11f, it is also observed that the I(A<sub>1</sub>(LO))/I(E<sub>2</sub><sup>high</sup>) of ZnO films is larger than that of Cu-doped ZnO film at the same H<sub>2</sub> flux, indicating that the amount of defects in the ZnO films is higher, as discussed above.

In addition to scattering peaks of E<sub>2</sub> and A<sub>1</sub>(LO) vibrational modes, it is also worth noting that there are scattering peaks around 135, 185 and 275 cm<sup>-1</sup>. The scattering peaks in range of 100–200 cm<sup>-1</sup> have been less reported in ZnO-based films, and they can be attributed to the acoustical phonons that are activated by incorporated impurities disturbing lattice [27,61,62]. In

this study, the amount of incorporated hydrogen increases and tends to saturate with the increase of  $H_2$  flux, as mentioned above. Thus, the appearance of scattering peaks around 135 and  $185\text{ cm}^{-1}$  is observed due to the incorporated hydrogen disturbing lattice after the  $H_2$  flux increases to 6 sccm for the ZnO and Cu-doped ZnO films. The appearance of scattering peak at around  $275\text{ cm}^{-1}$  is generally thought to be related to  $Zn_i$  in the films [63–65]. In the ZnO films, this peak can be observed at  $H_2$  flux of 0–18 sccm, which indicates that there is a high concentration of  $Zn_i$  in the films. For the Cu-doped ZnO films, the scattering peak at  $275\text{ cm}^{-1}$  can be observed at  $H_2$  flux above 3 sccm, which indicates that the concentration of  $Zn_i$  defects in the films is lower at  $H_2$  flux of 0–3 sccm and it becomes higher after  $H_2$  flux increases to 6 sccm. These results are basically consistent with the results of  $Zn_i$  content in the film obtained by XPS analysis.

Finally, it is worth mentioning that the current research results can lay the foundation for the further device application of the co-doped or hydrogen-doped ZnO films. For example, the defect amount and resistivity of the films can be adjusted over a wide range by Cu and/or hydrogen doping, which provides the possibility for the development of high-performance resistive random access memory (RRAM) and gas sensors [66,67]. The performance of ZnO-based thin film transistors (TFTs) could be improved by hydrogenation treatment due to the fact that hydrogen could act as a defect passivator and a shallow donor in ZnO-based films [68,69]. Thus, it is clear that co-doped or hydrogen-doped ZnO films prepared with different  $H_2$  fluxes may be used to make high-performance TFTs devices. The co-doped film or hydrogen-doped ZnO has adjustable  $E_g$ ,  $T_{vis}$ ,  $V_O$  and other defects, which provides conditions for the development of high-performance UV or visible light detectors [70]. The co-doped film may be a high-performance photocatalyst due to the enhancement of visible light absorption and the increase of  $Cu^+$  content in the film [71]. The co-doped film can exhibit strong ferromagnetism due to existence of a large amount of  $V_O$  and  $Cu^+$  in the films, making it suitable for use in spintronic devices [24]. In future, the device application of Cu and hydrogen co-doped or hydrogen-doped ZnO films in these fields will be further investigated.

#### IV. Conclusions

The structure and electrical-optical properties of ZnO and Cu-doped ZnO films can be tailored by  $H_2$  flux. With increase of  $H_2$  flux, film thickness decreases and surface roughness first increases and then decreases due to the etching effect of hydrogen plasma. Meanwhile, appropriate  $H_2$  flux can improve (002) preferred orientation and crystallinity of both films. The conduction properties of both films are enhanced at suitable  $H_2$  fluxes. Hydrogen doping can compensate the ac-

ceptor defects formed by Cu doping, so that the Cu-doped ZnO films with better conductive properties can be obtained at larger  $H_2$  fluxes. The electrical stability in air of the Cu-doped ZnO films is better than that of the ZnO films because of larger film thickness, lower  $V_O$  contents and easier formation of Cu–H and  $H_O$  defects. The instability of  $H_i$  causes a significant degradation in the conduction properties of both films after annealing. High  $H_2$  fluxes cause decrease of  $T_{vis}$  of the Cu-doped ZnO films because of high Cu content and thicker film thickness. Band gap energy ( $E_g$ ) of the films as a function of  $H_2$  flux is governed by Burstein-Moss (BM) effect. With increasing  $H_2$  flux,  $E_2^{high}$  and  $A_1(LO)$  scattering peaks of both films tend to enhance at first and then weaken, but their intensity ratio  $I(A_1(LO))/I(E_2^{high})$  tends to increase. The  $E_2^{high}$  and  $A_1(LO)$  scattering peaks are mainly controlled by film crystallinity and the content of defect such as  $V_O$ ,  $Zn_i$ , and  $H_i$  in the films, respectively. The appearance of scattering peaks around 135 and  $185\text{ cm}^{-1}$  can be ascribed to the incorporated hydrogen disturbing lattice, and the scattering peak around  $275\text{ cm}^{-1}$  is linked to the  $Zn_i$  content. At the same  $H_2$  flux, Cu doping leads to the lower  $E_g$  and  $I(A_1(LO))/I(E_2^{high})$  of Cu-doped ZnO films.

**Acknowledgements:** The authors gratefully acknowledge the support from the Opening Project of The State Key Laboratory of Refractories and Metallurgy (G202306). Dr. Zhang Guohong at the Analytical & Testing Center of Wuhan University of Science and Technology is also thanked for the help on XPS measurement.

#### References

1. I. Sugihartono, B. Soegijono, E. Handoko, T.S. Tiam, A.A. Umar, "Structure and optical properties of La-doped ZnO thin films at room temperature", *Process. Appl. Ceram.*, **17** [2] (2023) 107–112.
2. K. Ellmer, A. Klein, B. Rech, *Transparent Conductive Zinc Oxide - Basics and Applications in Thin Film Solar Cells*, Springer Nature, 2008.
3. M.A. Borysiewicz, "ZnO as a functional material, a review", *Crystals*, **9** (2019) 505.
4. I. Sugihartono, S.T. Tan, A. Arkundato, R. Fahdiran, I. Isnaeni, E. Handoko, S. Budi, A.S. Budi, "The effect of Al-Cu co-dopants on morphology, structure, and optical properties of ZnO nanostructures", *Mater. Res.*, **26** (2023) e20220499.
5. F. Xiu, J. Xu, P.C. Joshi, C.A. Bridges, M.P. Paranthaman, "ZnO doping and defect engineering - A review", pp. 105–140 in *Semiconductor materials for solar photovoltaic cells*. Eds. M. Paranthaman, W.N. Wong, R. Bhattacharya, Springer, 2016.
6. X.B. Wang, C. Song, K.W. Geng, F. Zeng, F. Pan, "Photoluminescence and Raman scattering of Cu-doped ZnO films prepared by magnetron sputtering", *Appl. Surf. Sci.*, **253** (2007) 6905–6909.
7. N.L. Tarwal, K.V. Gurav, S.H. Mujawar, S.B. Sadale, K.W.

- Nam, W.R. Bae, A.V. Moholkar, J.H. Kim, P.S. Patil, J.H. Jang, “Photoluminescence and photoelectrochemical properties of the spray deposited copper doped zinc oxide thin films”, *Ceram. Int.*, **40** (2014) 7669–7677.
8. M. Suja, S.B. Bashar, M.M. Morshed, J. Liu, “Realization of Cu-doped p-type ZnO thin films by molecular beam epitaxy”, *ACS Appl. Mater. Interfaces*, **7** (2015) 8894–8899.
  9. P. Khosravia, F. Karimzadeha, H.R. Salimijazia, Y. Abdib, “Structural, optical and electrical properties of co-sputtered p-type ZnO:Cu thin-films”, *Ceram. Int.*, **45** (2019) 7472–7479.
  10. D.L. Hou, X.J. Ye, X.Y. Zhao, H.J. Meng, H.J. Zhou, X.L. Li, C.M. Zhen, “Room-temperature ferromagnetism in n-type Cu-doped ZnO thin films”, *J. Appl. Phys.*, **102** (2007) 033905.
  11. Y.M. Hu, S.S. Li, C.H. Kuang, T.C. Han, C.C. Yu, “Post-annealing effect on the room-temperature ferromagnetism in Cu-doped ZnO thin films”, *J. Appl. Phys.*, **117** (2015) 17B901.
  12. C.G. Van de Walle, “Hydrogen as a cause of doping in zinc oxide”, *Phys. Rev. Lett.*, **85** (2000) 1012–1015.
  13. A. Janotti, C.G. Van de Walle, “Hydrogen multicentre bonds”, *Nat. Mater.*, **6** (2007) 44–47.
  14. D. Gaspar, L. Pereira, K. Gehrke, B. Galler, E. Fortunato, R. Martins, “High mobility hydrogenated zinc oxide thin films”, *Sol. Energ. Mat. Sol. C*, **163** (2017) 255–262.
  15. P.F. Cai, J.B. You, X.W. Zhang, J.J. Dong, X.L. Yang, Z.G. Yin, N.F. Chen, “Enhancement of conductivity and transmittance of ZnO films by post hydrogen plasma treatment”, *J. Appl. Phys.*, **105** (2009) 083713.
  16. Y. Hayashi, M. Arita, C.G. Lee, “The effects of hydrogen on the electrical and optical properties of ZnO”, *Int. J. Nucl. Hydrogen Prod. Appl.*, **2** (2009) 21–28.
  17. H. Akazawa, “Hydrogen induced electric conduction in undoped ZnO and Ga-doped ZnO thin films: Creating native donors via reduction, hydrogen donors, and reactivating extrinsic donors”, *J. Vac. Sci. Technol. A*, **32** (2014) 051511.
  18. B.L. Zhu, J. Wang, S.J. Zhu, J. Wu, D.W. Zeng, C.S. Xie, “Investigation of structural, electrical, and optical properties for Al-doped ZnO films deposited at different substrate temperatures and H<sub>2</sub> ratios”, *J. Electrochem. Soc.*, **159** (2012) H536–H544.
  19. P. Mondal, D. Das, “Effect of hydrogen in controlling the structural orientation of ZnO:Ga:H as transparent conducting oxide films suitable for applications in stacked layer devices”, *Phys. Chem. Chem. Phys.*, **18** (2016) 20450.
  20. J. Hu, B.C. Pan, “Formation and dissociation of a Cu-H complex in ZnO”, *J. Phys. Chem. C*, **112** (2008) 19142–19146.
  21. E.V. Lavrov, J. Weber, F. Borrner, C.G. Van de Walle, R. Helbig, “Hydrogen-related defects in ZnO studied by infrared absorption spectroscopy”, *Phys. Rev. B*, **66** (2002) 165205.
  22. M.G. Wardle, J.P. Goss, P.R. Briddon, “Theory of Fe, Co, Ni, Cu, and their complexes with hydrogen in ZnO”, *Phys. Rev. B*, **72** (2005) 155108.
  23. Z. Zhou, K. Kato, T. Komaki, M. Yoshino, H. Yukawa, M. Morinaga, K. Morita, “Electrical conductivity of Cu-doped ZnO and its change with hydrogen implantation”, *J. Electroceram.*, **11** (2003) 73–79.
  24. T. Li, W. Xiao, T.S. Herg, N. Bao, J. Ding, “Magnetic and optical studies of hydrogenated Cu-doped ZnO film”, *J. Korean Phys. Soc.*, **62** [12] (2013) 1738–1743.
  25. X. Cai, H.W. Liang, Y.D. Liu, R.S. Shen, Xi.H. Xia, Y. Liu, C.C. Ling, G.T. Du, “Study of the thermal stability of the H-related donors in high resistivity ZnO:Cu thin films by high-pressure H<sub>2</sub> treatment”, *Chem. Phys. Lett.*, **579** (2013) 90–93.
  26. B.L. Zhu, X.M. Cao, M. Xie, J. Wu, X.W. Shi, “Effects of Cu doping and deposition atmosphere on structural, electrical, optical and magnetic properties of ZnO films”, *Physica B*, **658** (2023) 414844.
  27. B.L. Zhu, J. Hu, M. Xie, J. Wu, X.W. Shi, “Structural, electrical, and optical properties of hydrogen and Cu codoped ZnO films prepared by magnetron sputtering at two substrate temperatures”, *Mater. Today Commun.*, **35** (2023) 106057.
  28. J.N. Duenow, T.A. Gessert, D.M. Wood, A.C. Dillon, T.J. Coutts, “Effects of hydrogen ambient and film thickness on ZnO:Al properties”, *J. Vac. Sci. Technol. A*, **26** (2008) 692–696.
  29. F.H. Wang, T.H. Yang, “Effect of hydrogen doping on the properties of Al and F co-doped ZnO films for thin film silicon solar cell applications”, *Thin Solid Films*, **605** (2016) 64–72.
  30. Y.F. Wang, Q. Huang, C.C. Wei, D.K. Zhang, Y. Zhao, X.D. Zhang, “Improvement of electrical and optical properties of molybdenum doped zinc oxide films by introducing hydrogen”, *Appl. Surf. Sci.*, **258** (2012) 8797–8801.
  31. R.S. Mohar, I. Sugihartono, V. Fauzia, A.A. Umar, “Dependence of optical properties of Mg-doped ZnO nanorods on Al dopant”, *Surf. Interfaces*, **19** (2020) 100518.
  32. P.S. Vachhani, A.K. Bhatnagar, “Oxygen pressure-dependent band gap modification in Cu-doped and undoped ZnO films”, *Phys. Scripta*, **87** (2013) 045702.
  33. B.L. Zhu, S.J. Zhu, J. Wang, J. Wu, D.W. Zeng, C.S. Xie, “Thickness effect on structure and properties of ZAO thin films by RF magnetron sputtering at different substrate temperatures”, *Physica E*, **43** (2011) 1738–1745.
  34. V. Tvarozek, I. Novotny, P. Sutta, S. Flickyngerova, K. Schtereve, E. Vavrinsky, “Influence of sputtering parameters on crystalline structure of ZnO thin films”, *Thin Solid Films*, **515** (2007) 8756–8760.
  35. B.L. Zhu, K. Lv, J. Wang, T.T. Li, J. Wu, D.W. Zeng, C.S. Xie, “Characteristics of Al-doped ZnO thin films prepared in Ar+H<sub>2</sub> atmosphere and their vacuum annealing behaviour”, *J. Vac. Sci. Technol. A*, **31** (2013) 061513.
  36. Y.R. Park, J. Kim, Y.S. Kim, “Growth and characteristics of hydrogenated In-doped ZnO thin films by pulsed DC magnetron sputtering”, *Appl. Surf. Sci.*, **256** (2009) 1589–1594.
  37. J.H. Huang, C.P. Liu, “The influence of magnesium and hydrogen introduction in sputtered zinc oxide thin films”, *Thin Solid Films*, **498** (2006) 152–157.
  38. F.H. Wang, H.P. Chang, C.C. Tseng, C.C. Huang, “Effects of H<sub>2</sub> plasma treatment on properties of ZnO:Al thin films prepared by RF magnetron sputtering”, *Surf. Coat. Technol.*, **205** (2011) 5269–5277.
  39. Y.S. Kang, H.Y. Kim, J.Y. Lee, “Effects of hydrogen on the structural and electro-optical properties of zinc oxide thin films”, *J. Electrochem. Soc.*, **147** (2000) 4625–4629.
  40. C.H. Liang, W.S. Hwang, “Stability of the electro-optical properties and structural characteristics of H and Al codoped ZnO films after heat treatment in H/Ar plasma”, *Ceram. Int.*, **40** (2014) 11857–11868.

41. L. Ma, S. Ma, H. Chen, X. Ai, X. Huang, “Microstructures and optical properties of Cu-doped ZnO films prepared by radio frequency reactive magnetron sputtering”, *Appl. Surf. Sci.*, **257** (2011) 10036–10041.
42. A.T.T. Pham, D.V. Hoang, T.H. Nguyen, O.K.T. Le, D.P. Wong, J.L. Kuo, K.H. Chen, T.B. Phan, V.C. Tran, “Hydrogen enhancing Ga doping efficiency and electron mobility in high-performance transparent conducting Ga-doped ZnO films”, *J. Alloys Compd.*, **860** (2020) 158518.
43. F. Bocchese, D. Cornil, E. Haye, J. Cornil, S. Lucas, “Three-zone model for Ti, Al co-doped ZnO films deposited by magnetron sputtering”, *Surf. Interfaces*, **28** (2022) 101595.
44. P. Qiu, Y. Lai, X. Sun, C. Chen, L. Ge, “Potent n-type nanostructured cruciate flower-like Cu/Cu<sub>2</sub>O films for photocathodic protection”, *Mater. Chem. Phys.*, **241** (2020) 122311.
45. R. Groenen, M. Creatore, M.C.M. van de Sanden, “Dry etching of surface textured zinc oxide using a remote argon–hydrogen plasma”, *Appl. Surf. Sci.*, **241** (2005) 321–325.
46. W.W. Liu, B. Yao, Y.F. Li, B.H. Li, Z.Z. Zhang, C.X. Shan, D.X. Zhao, J.Y. Zhang, D.Z. Shen, X.W. Fan, “Structure, luminescence and electrical properties of ZnO thin films annealed in H<sub>2</sub> and H<sub>2</sub>O ambient: A comparative study”, *Thin Solid Films*, **518** (2010) 3923–3928.
47. S.Y. Myong, S.I. Park, K.S. Lim, “Improvement of electrical stability of polycrystalline ZnO thin films via intentional post-deposition hydrogen doping”, *Thin Solid Films*, **513** (2006) 148–151.
48. B. Sang, A. Yamada, M. Konagai, “Highly stable ZnO thin films by atomic layer deposition”, *Jpn. J. Appl. Phys.*, **37** (1998) L1125–L1128.
49. J. Bang, K.J. Chang, “Diffusion and thermal stability of hydrogen in ZnO”, *Appl. Phys. Lett.*, **92** (2008) 132109.
50. C.A. Wolden, T.M. Barnes, J.B. Baxter, E.S. Aydil, “Infrared detection of hydrogen-generated free carriers in polycrystalline ZnO thin films”, *J. Appl. Phys.*, **97** (2005) 043522.
51. S.J. Jokela, M.D. McCluskey, “Structure and stability of O-H donors in ZnO from high-pressure and infrared spectroscopy”, *Phys. Rev. B*, **72** (2005) 113201.
52. B.L. Zhu, J.M. Ma, K. Lv, C.J. Wang, J. Wu, Z.H. Gan, J. Liu, X.W. Shi, “Improvement of transparent conductive properties of GZO/Cu/GZO tri-layer films by introducing H<sub>2</sub> into sputtering atmosphere”, *Superlattice Microst.*, **140** (2020) 106456.
53. K.S. Ahn, T. Deutsch, Y. Yan, C.S. Jiang, C.L. Perkins, J. Turner, M. Al-Jassim, “Synthesis of band-gap-reduced p-type ZnO films by Cu incorporation”, *J. Appl. Phys.*, **102** (2007) 023517.
54. T.C. Damen, S.P.S. Porto, B. Tell, “Raman effect in zinc oxide”, *Phys. Rev.*, **142** (1966) 570–574.
55. C. Lung, M. Toma, M. Pop, D. Marconi, A. Pop, “Characterization of the structural and optical properties of ZnO thin films doped with Ga, Al and (Al + Ga)”, *J. Alloys Compd.*, **725** (2017) 1238–1243.
56. E. Muchuweni, T.S. Sathiaraj, H. Nyakoty, “Effect of O<sub>2</sub>/Ar flow ratio on Ga and Al co-doped ZnO thin films by rf sputtering for optoelectronic device fabrication”, *Mater. Res. Bull.*, **95** (2017) 123–128.
57. S. Singh, T. Ganguli, R. Kumar, R.S. Srinivasa, S.S. Major, “Substrate temperature dependence of growth mode, microstructure and optical properties of highly oriented zinc oxide films deposited by reactive sputtering”, *Thin Solid Films*, **517** (2008) 661–669.
58. Y. Hu, Y. Chen, J. Chen, X. Chen, D. Ma, “Effects of hydrogen flow on properties of hydrogen doped ZnO thin films prepared by RF magnetron sputtering”, *Appl. Phys. A*, **114** (2014) 875–882.
59. Y.R. Park, J. Kim, Y.S. Kim, “Effect of hydrogen doping in ZnO thin films by pulsed DC magnetron sputtering”, *Appl. Surf. Sci.*, **255** (2009) 9010–9014.
60. J. Ye, S. Gu, S. Zhu, T. Chen, W. Liu, F. Qin, L. Hu, R. Zhang, Y. Shi, Y. Zheng, “Raman and photoluminescence of ZnO films deposited on Si (111) using low-pressure metalorganic chemical vapor deposition”, *J. Vac. Sci. Technol. A*, **21** (2003) 979–982.
61. R. Kirste, Y. Aksu, M.R. Wagner, S. Khachadorian, S. Jana, M. Driess, C. Thomsen, A. Hoffmann, “Raman and photoluminescence spectroscopic detection of surface-bound Li<sup>+</sup>O<sub>2</sub><sup>-</sup> defect sites in Li-doped ZnO nanocrystals derived from molecular precursors”, *ChemPhysChem*, **12** (2011) 1189–1195.
62. H.K. Yadav, K. Sreenivas, V. Gupta, J.F. Scott, R.S. Katiyar, “Raman spectroscopy and dielectric studies of multiple phase transitions in ZnO:Ni”, *Appl. Phys. Lett.*, **92** (2008) 122908.
63. M.A. Gluba, N.H. Nickel, N. Karpensky, “Interstitial zinc clusters in zinc oxide”, *Phys. Rev. B*, **88** (2013) 245201.
64. H. Zhang, W.J. Li, G.P. Qin, H.B. Ruan, Z. Huang, F. Wu, C.Y. Kong, L. Fang, “Role of zinc interstitial defects in indium and magnesium codoped ZnO transparent conducting films”, *Appl. Surf. Sci.*, **492** (2019) 392–398.
65. A.V. Vasin, A.V. Rusavsky, E.G. Bortchagovsky, Y.V. Gomeniuk, A.S. Nikolenko, V.V. Strelchuk, R. Yatskiv, S. Tiagulskyi, S. Prucnal, W. Skorupa, A.N. Nazarov, “Methane as a novel doping precursor for deposition of highly conductive ZnO thin films by magnetron sputtering”, *Vacuum*, **174** (2020) 109199.
66. C.H. Jia, Q.C. Dong, W.F. Zhang, “Effect of incorporating copper on resistive switching properties of ZnO films”, *J. Alloys Compd.*, **520** (2012) 250–254.
67. K.G. Giriya, K. Somasundaram, A. Topkar, R.K. Vatsa, “Highly selective H<sub>2</sub>S gas sensor based on Cu-doped ZnO nanocrystalline films deposited by RF magnetron sputtering of powder target”, *J. Alloys Compd.*, **684** (2016) 15–20.
68. L. Xu, Q. Chen, L. Liao, X.Q. Liu, T.C. Chang, K.C. Chang, T.M. Tsai, C.Z. Jiang, J.L. Wang, J.C. Li, “Rational hydrogenation for enhanced mobility and high reliability on ZnO-based thin film transistors: From simulation to experiment”, *ACS Appl. Mater. Inter.*, **8** (2016) 5408–5415.
69. D.L. Zhu, Z.J. Jiang, W.H. Zhang, D.B. Yin, W.Y. Xu, S. Han, M. Fang, W.J. Liu, P.J. Cao, Y.M. Lu, “Room-temperature fabrication of high-performance H doped ZnO thin-film transistors”, *Mater. Chem. Phys.*, **261** (2021) 124248.
70. P.S. Shewale, Y.S. Yu, “UV photodetection properties of pulsed laser deposited Cu-doped ZnO thin film”, *Ceram. Int.*, **43** (2017) 4175–4182.
71. P. Jongnavakit, P. Amornpitoksuk, S. Suwanboon, N. Ndiege, “Preparation and photocatalytic activity of Cu-doped ZnO thin films prepared by the sol-gel method”, *Appl. Surf. Sci.*, **258** (2012) 8192–8198.